



LAWRENCE  
LIVERMORE  
NATIONAL  
LABORATORY

# Multi-model mean nitrogen and sulfur deposition from the Atmospheric Chemistry and Climate Model Intercomparison Project (ACCMIP): evaluation of historical and projected future

J. F. Lamarque, F. Dentener, J. McConnell, C. U. Ro, M. Shaw, R. Vet, D. Bergmann, P. Cameron-Smith, S. Dalsoren, R. Doherty, G. Faluvegi, S. J. Ghan, B. Josse, Y. H. Lee, I. A. MacKenzie, D. Plummer, D. T. Shindell, R. B. Skeie, D. S. Stevenson, S. Strode, G. Zeng, M. Curran, D. Dahl-Jensen, S. Das, D. Fritzsche, M. Nolan

October 2, 2013

Atmospheric Chemistry and Physics

## **Disclaimer**

---

This document was prepared as an account of work sponsored by an agency of the United States government. Neither the United States government nor Lawrence Livermore National Security, LLC, nor any of their employees makes any warranty, expressed or implied, or assumes any legal liability or responsibility for the accuracy, completeness, or usefulness of any information, apparatus, product, or process disclosed, or represents that its use would not infringe privately owned rights. Reference herein to any specific commercial product, process, or service by trade name, trademark, manufacturer, or otherwise does not necessarily constitute or imply its endorsement, recommendation, or favoring by the United States government or Lawrence Livermore National Security, LLC. The views and opinions of authors expressed herein do not necessarily state or reflect those of the United States government or Lawrence Livermore National Security, LLC, and shall not be used for advertising or product endorsement purposes.

# Multi-model mean nitrogen and sulfur deposition from the Atmospheric Chemistry and Climate Model Intercomparison Project (ACCMIP): evaluation of historical and projected future changes

J.-F. Lamarque<sup>1</sup>, F. Dentener<sup>2</sup>, J. McConnell<sup>3</sup>, C.-U. Ro<sup>4</sup>, M. Shaw<sup>4</sup>, R. Vet<sup>4</sup>, D. Bergmann<sup>5</sup>, P. Cameron-Smith<sup>5</sup>, S. Dalsoren<sup>6</sup>, R. Doherty<sup>7</sup>, G. Faluvegi<sup>8</sup>, S. J. Ghan<sup>9</sup>, B. Josse<sup>10</sup>, Y. H. Lee<sup>8</sup>, I. A. MacKenzie<sup>7</sup>, D. Plummer<sup>11</sup>, D. T. Shindell<sup>8</sup>, R. B. Skeie<sup>6</sup>, D. S. Stevenson<sup>7</sup>, S. Strode<sup>12,13</sup>, G. Zeng<sup>14</sup>, M. Curran<sup>15</sup>, D. Dahl-Jensen<sup>16</sup>, S. Das<sup>17</sup>, D. Fritzsche<sup>18</sup>, and M. Nolan<sup>19</sup>

<sup>1</sup>NCAR Earth System Laboratory, National Center for Atmospheric Research, Boulder, CO, USA

<sup>2</sup>European Commission, Joint Research Centre, Ispra, Italy

<sup>3</sup>Desert Research Institute, Reno, NV, USA

<sup>4</sup>Environment Canada, Toronto, Ontario, Canada

<sup>5</sup>Lawrence Livermore National Laboratory, Livermore, CA, USA

<sup>6</sup>Center for International Climate and Environmental Research-Oslo (CICERO), Oslo, Norway

<sup>7</sup>School of GeoSciences, University of Edinburgh, Edinburgh, UK

<sup>8</sup>NASA Goddard Institute for Space Studies and Columbia Earth Institute, New York, NY, USA

<sup>9</sup>Pacific Northwest National Laboratory, Richland, WA, USA

<sup>10</sup>GAME/CNRM, Météo-France, CNRS – Centre National de Recherches Météorologiques, Toulouse, France

<sup>11</sup>Canadian Centre for Climate Modeling and Analysis, Environment Canada, Victoria, British Columbia, Canada

<sup>12</sup>NASA Goddard Space Flight Center, Greenbelt, MD, USA

<sup>13</sup>Universities Space Research Association, Columbia, MD, USA

<sup>14</sup>National Institute of Water and Atmospheric Research, Lauder, New Zealand

<sup>15</sup>Australian Antarctic Division and Antarctic Climate & Ecosystems CRC, Hobart, Tasmania, Australia

<sup>16</sup>Niels Bohr Institute, University of Copenhagen, Copenhagen, Denmark

<sup>17</sup>Woods Hole Oceanographic Institution, Woods Hole, MA, USA

<sup>18</sup>Alfred Wegener Institute, Helmholtz Centre for Polar and Marine Research, Research Unit Potsdam, Germany

<sup>19</sup>University of Alaska Fairbanks, Fairbanks, AK, USA

*Correspondence to:* J.-F. Lamarque (lamar@ucar.edu)

**Abstract.** We present multi-model global datasets of nitrogen and sulfate deposition covering time periods from 1850 to 2100, calculated within the Atmospheric Chemistry and Climate Model Intercomparison Project (ACCMIP). The computed deposition fluxes are compared to surface wet deposition and ice-core measurements. We use a new dataset of wet deposition for 2000–2002 based on critical assessment of the quality of existing regional network data. We show that for present-day (year 2000 ACCMIP time-slice), the ACCMIP results perform similarly to previously published

multi-model assessments. For this time slice, we find a multi-model mean deposition of approximately 50 Tg(N) yr<sup>-1</sup> from nitrogen oxide emissions, 60 Tg(N) yr<sup>-1</sup> from ammonia emissions, and 83 Tg(S) yr<sup>-1</sup> from sulfur emissions. The analysis of changes between 1980 and 2000 indicates significant differences between model and measurements over the United States but less so over Europe. This difference points towards a potential misrepresentation of 1980 NH<sub>3</sub> emissions over North America. Based on ice-core records, the 1850 deposition fluxes agree well with Greenland ice

cores but the change between 1850 and 2000 seems to be overestimated in the Northern Hemisphere for both nitrogen and sulfur species. Using the Representative Concentration Pathways (RCPs) to define the projected climate and atmospheric chemistry related emissions and concentrations, we find large regional nitrogen deposition increases in 2100 in Latin America, Africa and parts of Asia under some of the scenarios considered. Increases in South Asia are especially large, and are seen in all scenarios, with 2100 values more than double their 2000 counterpart in some scenarios and reaching  $> 1300 \text{ mg(N) m}^{-2} \text{ yr}^{-1}$  averaged over regional to continental scale regions in RCP 2.6 and 8.5,  $\sim 30\text{--}50\%$  larger than the values in any region currently (*circa* 2000). On the other hand, sulfur deposition rates in 2100 are in all regions lower than in 2000 in all the RCPs. The new ACCMIP multi-model deposition dataset provides state-of-the-science, consistent and evaluated time slice (spanning 1850–2100) global gridded deposition fields for use in a wide range of climate and ecological studies.

## 1 Introduction

The global nitrogen cycle is of importance for a number of key-issues, such as ecology and biodiversity (e.g. Phoenix et al., 2006; Bobbink et al., 2010; Butchart et al., 2010), eutrophication and acidification (e.g. Bouwman et al., 2002; Rodhe et al., 2002; Fisher et al., 2011), climate change-carbon cycle interactions (e.g. Thornton et al., 2007; Reay et al., 2008; Zaehle et al. 2010), food and energy production (Sutton et al., 2011). Nitrogen emissions also impact human health through particulate matter and ozone formation. Clearly, nitrogen is central to many aspects of life on Earth (Galloway et al., 2008; Fowler et al., 2013). Similarly, sulfur is an essential nutrient but excessive sulfur deposition has been linked to a decrease in tree growth as a result of soil acidification and modification to plant nutrition and soil chemistry (Savva and Berninger, 2010).

Dinitrogen ( $\text{N}_2$ ) is the most abundant component in the atmosphere, but is chemically unreactive. More reactive atmospheric nitrogen components include oxidized  $\text{NO}_y$  ( $= \text{NO} + \text{NO}_2$  + other minor inorganic components and organic nitrogens), the long-lived greenhouse gas dinitrous oxide ( $\text{N}_2\text{O}$ ; with a lifetime of  $131 \pm 10 \text{ yr}$ , Prather et al., 2012), and reduced nitrogen  $\text{NH}_x$  ( $= \text{NH}_3 + \text{NH}_4^+$ ) as well as organic nitrogen components such as amines (Kanakidou et al., 2012) or organic nitrates. Deposited  $\text{SO}_x$  ( $= \text{SO}_2 + \text{SO}_4^{2-}$ ) sulfur compounds originate from emissions of  $\text{SO}_2$ , sulfate and dimethyl sulfide.

Anthropogenic emissions of  $\text{NO}_y$ ,  $\text{NH}_x$  and  $\text{SO}_x$  components are estimated to have increased by a factor of 5 to 10 since 1850 (van Aardenne et al., 2001; Lamarque et al., 2010). Knowledge of the link between their generation by human activities and subsequent transformations and impacts requires an accurate description of large scale emissions, at-

mospheric chemistry transport and removal, all of which occur on relatively fast timescales (up to a few weeks) compared to nitrogen in the other compartments of relevance to the Earth system: terrestrial, coastal zones and open ocean.

Global atmospheric-chemistry transport models are routinely used as a tool to calculate the global dispersion of  $\text{NO}_y$ ,  $\text{NH}_x$  and  $\text{SO}_x$ . Since individual models are prone to specific errors and multi-model means typically outperform individual models (e.g. Reichler and Kim, 2008; Shindell et al., 2013), it has become common to use model ensemble calculations to improve the quality of the calculations. Previous deposition ensemble studies include Lamarque et al. (2005) using 6 models and focusing on  $\text{NO}_y$  deposition, Dentener et al. (2006) using 23 models and discussing  $\text{NO}_y$ ,  $\text{NH}_x$  and  $\text{SO}_x$  deposition under current and 2 future scenarios, and Sanderson et al. (2008) using 15 models and focusing on export of  $\text{NO}_y$  and subsequent deposition.

The present study uses deposition fields generated by 11 models that participated in the Atmospheric Chemistry and Climate Model Intercomparison Project (ACCMIP; Lamarque et al., 2013). ACCMIP was designed to inform aspects of the forthcoming Intergovernmental Panel on Climate Change Assessment Report #5 regarding the role of long-term changes in atmospheric chemistry on climate and vice-versa. In this ACCMIP study simulations were provided for time slices representative of the period around 1850, 1980, 2000, 2030 and 2100 (see Sect. 2), where the future atmospheric chemistry-climate conditions follow the 4 Representative Concentration Pathways (RCPs, Moss et al., 2010). Because of the importance of sulfur deposition (in association with nitrogen deposition) for the understanding of soil and water acidification (Fisher et al., 2011), we have included an analysis of sulfur deposition to the more traditional nitrogen deposition analysis. The models used in this analysis represent a combination of the current generation of Chemistry-Transport Models and Chemistry-Climate Models, with somewhat refined horizontal (ranging from  $1.875 \times 2.5$  degrees to  $5 \times 5$  degrees) and vertical resolution (from 19 to 72 levels) and more detailed descriptions of chemical processes compared to previous studies (namely the results discussed in Dentener et al., 2006; Sanderson et al., 2008). Rather than representing specific meteorological years – as in these previous studies – each model meteorology (generated by climate models) is representative in a climatic sense of the decade under consideration (e.g. 1850–1859; or 2000–2009) and hence include the effect of climate change.

This paper is structured as follows. Section 2 gives a short description of the models and the ACCMIP experiments. We also define there the methodology for computing the multi-model mean (MMM). Section 3 describes the measurement datasets used in this paper, from surface sites and from ice cores. In Sect. 4, we evaluate the multi-model mean for the 2000 period – when extensive measured deposition datasets are available, and which allows us also to make a retrospec-

tive analysis of the quality of data in this model dataset compared to the earlier and widely used Photocomp (Dentener et al., 2006) and HTAP (Sanderson et al., 2008; Vet et al., 2013) deposition datasets. In Sect. 5, a more limited analysis is given for the changes in deposition (and its drivers) since the 1980s. In Sect. 6, using ice-cores, we evaluate the simulated change between decades centered around 1850 and 2000. The 1980–2000 period is of particular interest since, due to implementation of national and international emission control measures, strong emission reductions have been reported, especially over North America and Europe, with commensurate consequences for deposition. Section 7 describes the overall global structure of total deposition (dry and wet) from 1850 to 2100. A discussion and conclusions follow in Sect. 8.

## 2 ACCMIP simulations and multi-model mean

An overview of the Atmospheric Chemistry and Climate Model Intercomparison Project (ACCMIP) simulations and participating models is given in Lamarque et al. (2013). Consequently, we focus here on the aspects relevant to the analysis of nitrogen and sulfate deposition.

ACCMIP provides analysis on the role of atmospheric chemistry changes in the near-term (up to 2100) climate forcing included in the CMIP5 (Climate Model Intercomparison Project Phase 5; Taylor et al., 2012) simulations, including the chemical composition changes associated with the CMIP5 prescribed forcings. The ACCMIP simulations used in the present study (Table 1) consist of time slice experiments (for specific periods spanning 1850 to 2100 with a minimum increment of 10 yr) with chemistry diagnostics. Each requested simulation is labeled as Primary (“P”) or Optional (“O”). Although simulations using the Representative Concentration Pathway 6.0 (RCP6.0, Masui et al., 2011) emissions were performed, not enough groups provided the necessary fields for a meaningful analysis of nitrogen and sulfur depositions; therefore, this work focuses on the remaining three RCP projections RCP2.6, RCP4.5 and RCP8.5 (see van Vuuren et al., 2011 and references therein). A primary output of these simulations was nitrogen and sulfate (dry and wet) deposition fields (see Table S1 in Lamarque et al., 2013). Although the ACCMIP models were required to specify the anthropogenic and biomass burning emissions according to Lamarque et al. (2010) for 1850–2000 and the RCP emissions (van Vuuren et al., 2011) beyond 2000, there is a range of emissions that were used in ACCMIP models, mostly from variations in the treatment of natural emissions (Lamarque et al., 2013; Young et al., 2013).

As a first step in the quality control of the model calculated depositions, we analyze for each model the balance between emission and deposition as reported by the modeling groups (Tables 2–4) for the year 2000 time slice experiment. This analysis is done separately for nitrogen orig-

inating from nitrogen oxide emissions (deposition fields are referred as a group as  $\text{NO}_y$ ) or ammonia emissions ( $\text{NH}_x$ ) and sulfur emissions ( $\text{SO}_x$ ). We find that the  $\text{NO}_y$  deposition is larger than the emissions (surface and upper-air, including lightning) by approximately  $1 \text{ Tg(N) yr}^{-1}$ , representing the input of nitrogen (mostly in the form of nitric acid) from the stratosphere, in general agreement with observational estimates of  $0.45 \text{ Tg(N) yr}^{-1}$  from Murphy and Fahey (1998), except for the GISS model where this influx is approximately  $5 \text{ Tg(N) yr}^{-1}$  and the CMAM and MOCAGE models where the balance between deposition and emission is achieved within round-off. In the case of ammonia, the balance between emissions and deposition is clearly attained. In the case of sulfur, this balance cannot be fully evaluated due to the lack of diagnostics on the formation of sulfate aerosols from the emitted dimethylsulfide (DMS). Boucher et al. (2003) estimated the yield (DMS to sulfate aerosols) to be 87% when both gas-phase and aqueous-phase reactions are taken into account, but this number will be somewhat model dependent. Within that limitation, we assume that balance between sulfur deposition and emission is achieved for the listed models.

The focus of this paper is on documenting the multi-model mean (MMM) generated for each time slice. The MMM is constructed by linearly interpolating the model generated monthly fields (for example wet deposition combined for all  $\text{NO}_y$  species) at their native horizontal resolution (Table S1) to a common  $0.5^\circ \times 0.5^\circ$  grid (finer than any model grid), identical to the emission grid used in Lamarque et al. (2010). Then, each field is averaged across models at the original monthly temporal resolution to generate its multi-model mean and standard deviation (Tables S2–S4). As indicated in these tables, the largest number of models (up to 10) that generated the necessary fields was for the historical  $\text{NO}_y$  deposition (Table S5), followed by the RCP8.5 simulations. The number of models performing ammonium chemistry and deposition is however much smaller (2–5 models, depending on the simulated time period) while between 2 and 7 models have provided sulfate fields. In all cases, the MMM is constructed using all available model results (Table S5), therefore leading to variations between the various models used in the average.

## 3 Description of observational deposition data

Under the auspices of the World Meteorological Organization (WMO) a precipitation chemistry expert group has performed a critical analysis of available wet deposition data for the years 2000 to 2002. While dry deposition may be available at specific sites, this is not a directly observed quantity and we therefore do not use this information. We use the WMO-processed wet deposition dataset in our analysis of the performance of the MMM in the 2000 time slice.

In this dataset, a careful analysis of worldwide reported data of wet precipitation chemistry was made, and data quality qualifiers are provided to deposition data obtained mainly from networks in Europe (European Monitoring and Evaluation Programme, EMEP; <http://www.nilu.no/projects/ccc/emepdata.html>); the United States (National Atmospheric Deposition Program, NADP; <http://nadp.sws.uiuc.edu/NTN/ntnData.aspx>); Canada (Canadian Air and Precipitation Monitoring Network, CAPMoN; <http://www.ec.gc.ca/rs-mn/default.asp?lang=En&n=752CE271-1>); Asia (mainly from the Acid Deposition Monitoring Network in East Asia EANET; <http://www.eanet.cc>), and Africa (Deposition of Biogeochemically Important Trace Species (DEBITS), <http://debts.sedoo.fr>). The evaluated wet deposition datasets, soon to be available through the World Data Centre for Precipitation Chemistry, only contain a subset of the available stations for that period, i.e. stations that correspond to regionally representative sites that fulfilled specific quality measures. In this paper, we use the wet deposition measurements of nitrate ( $\text{NO}_3^-$ ), ammonium ( $\text{NH}_4^+$ ) and non-sea salt sulfate ( $\text{SO}_4^{2-}$ ), which were accepted as ‘satisfactory’ or ‘conditional’ based on a quality assurance review that included expert assessments of measurement methods (wet-only versus bulk sampling, availability of precipitation gauge data, short sample collection periods) and data completeness statistics (annual percent coverage length of precipitation measurements, annual percent of total precipitation measured, and number of years included in the 3-year average) as specified in the World Meteorological Organization Global Atmosphere Watch Manual for the GAW Precipitation Chemistry Programme (WMO/GAW, 2004). All data are representative of regional, non-urban, non-suburban, non-industrial sites of the aforementioned networks, many of which are located in remote regions of the world. For more detailed information on data networks, data selection criteria, and an application to the HTAP Phase 1 deposition dataset, we refer to Vet et al. (2013), as well as the data networks indicated above. We will focus our present analysis on the NADP, EMEP and EANET observations. This choice was made for consistency with previous analysis (e.g. Dentener et al., 2006) but also for the higher degree of coverage over those regions.

Over Europe (EMEP) and the United States (NADP), deposition measurement sites typically started around the 1980s. We use these early measurements to evaluate the change in deposition over these two decades. To this purpose, we computed from the raw data (available at the aforementioned web sites), and using the filtering protocols defined by the specific networks, two sets of 6-yr averages (1980–1985 and 1997–2002 data) for sites that had sufficient observations for both time slices.

Although a quality control similar to the WMO evaluation was not available for the 1980s data, comparison of the WMO processed 2000–2002 data with our 1997–2002 indicate very good agreement over the respective regions (not

shown), validating the suitability of our processed dataset to study changes in deposition from the 1980s to the 2000s.

Historical records of nitrate, ammonium, and sulfur were also developed from high-depth-resolution measurements in ice cores (see Table S6 for their geographical information) using an established continuous ice core analytical system (e.g., McConnell and Edwards, 2008). Nitrate and ammonium were measured using spectrophotometry and fluorimetry, respectively, with standard flow through methods (Roethlisberger et al., 2000). Total sulfur concentrations were measured using magnetic sector Inductively Coupled Plasma Mass Spectrometry (McConnell and Edwards, 2008). At core sites with sufficient annual snowfall, the ice core records were dated using annual layer counting of a range of seasonally varying chemical species (Sigl et al., 2013). Synchronization to well-known volcanic layers was used for dating at core sites with very low snowfall (e.g., East Antarctica) where annual layers are not preserved (Anschütz et al., 2011) or at lower elevation sites (e.g., Akademii Nauk, McCall Glacier, Flade Isblink) where surface melting and percolation make annual layer identification difficult (Opel et al., 2009). Uncertainty ( $1\sigma$ ) in the dating is estimated at  $\pm 1$  yr for the annually dated sites and  $\pm 3$  yr for all other sites. Decadal averages centered on 1855 and 2000 were computed from the high-resolution measurements.

#### 4 Evaluation of ACCMIP year 2000 time slice deposition

While observation and model data are available at the monthly time resolution, we focus our analysis on the annual mean. This choice is made to limit the discussion to the long-term changes in nitrogen and sulfate deposition. In addition to the present intercomparison project, MMM results from two previous studies are available for comparison and analysis of potential improvements: PhotoComp (Dentener et al., 2006) and HTAP (Sanderson et al., 2012; Vet et al., 2013). These previous studies are partially independent of the present one, with different emissions and a different set of models or different versions of the same models. Using the WMO dataset and the model results interpolated to the location of the observing stations, we can statistically analyze the ability of the models to reproduce the observations.

We display in Fig. 1 the global and regional distributions of  $\text{NO}_3^-$  (Fig. 1a),  $\text{NH}_4^+$  (Fig. 1b) and  $\text{SO}_4^{2-}$  (Fig. 1c) wet deposition in the MMM compared to the WMO dataset (over Europe and the United States). Deposition is clearly strongly correlated with emissions (i.e. largest in the Northern Hemisphere, but also with larger amounts in areas of biomass burning and large soil emissions such as Central Africa), albeit with significant downwind propagation for each compound. Unlike the nitrogen sources, sulfur emissions from degassing volcanoes (Andres and Kasgnoc, 1998) lead to the

formation of deposition hotspots in areas with low anthropogenic emission levels such as Central America.

In the case of  $\text{NO}_3^-$  deposition, we find that all 3 experiments (ACCMIP, HTAP and PhotoComp) perform rather similarly (Fig. 2a and Table 5), with correlation coefficients between 0.8 and 0.9 over the North America and mean biases ranging from 10 to 20 %. However, none of those model simulations are able to capture the observed high deposition rates over East Asia or Europe, possibly due to the proximity of the observing stations to significant sources, features that cannot easily be captured with the coarse grid of presently used models (Zhang et al., 2012). In contrast, in the high emission region of Northeastern United States, there are regions of overestimation as well as underestimation.

In the case of  $\text{NH}_4^+$ , the ACCMIP results are slightly lower than the previous studies over both the North American NADP and European EMEP domains and therefore with a larger negative bias (-8 % instead of 3–6 %). Because of errors in the regridding of the  $\text{NH}_3$  agricultural emissions over China in ACCMIP (see <http://www.iiasa.ac.at/web-apps/tnt/RcpDb/dsd?Action=htmlpage&page=download>), the performance in ACCMIP (Fig. 2b and Table 5) is considerably worse than the previous studies over Asia, with a correlation coefficient of 0.2 instead of 0.8 for the PhotoComp and HTAP and a significant underestimate (by approximately 30 to 50 %, see Fig. 2b) for the highest deposition rates over East Asia. Furthermore, because the mapping error involves both China and Mongolia, there is an overestimation of nitrogen deposition from  $\text{NH}_x$  in that region. However no stations are available to provide an estimate of the bias.

The sulfate ( $\text{SO}_4^{2-}$ ) deposition (Fig. 2c and Table 5) is somewhat improved in ACCMIP over the NADP stations (with a mean bias of -6 % instead of 15 %), while the positive bias previously found in the HTAP dataset (12 %) over the EMEP domain is now reversed, so that the ACCMIP models are actually underestimating wet deposition over that region (-30 %). The deposition over EANET is characterized by a larger negative bias in ACCMIP than PhotoComp or HTAP (-42 % instead of -25 % to -32 %), although the overall correlation remains high (0.8–0.9).

Overall, the performance of the ACCMIP MMM is similar to PhotoComp and HTAP, suggesting that no significant improvement or worsening has been made since those 2 studies in the representation of emissions, chemical processing and deposition processes. The analysis also shows that ammonium deposition over East Asia is most likely underestimated. On the other hand, for all considered species, the ACCMIP MMM deposition tends to be lower than observed over the EMEP stations.

## 5 Evaluation of deposition changes: 1980–2000

To identify potential changes in deposition over time, we use the 1980 and 2000 time slice experiments. Unfortunately,

neither HTAP nor PhotoComp provide historical time slices and therefore such changes cannot be discussed within that context. Over that period, Europe and North America have seen significant changes in nitrogen and sulfur emissions, from a combination of changes in anthropogenic activities and air quality regulations (Granier et al., 2011; Xing et al., 2012).

To limit issues associated with interannual variability (not captured by the ACCMIP model simulations) and uneven time sampling from the observed wet deposition rates, we only select stations with at least 36 months of available data for each 6-yr averaging period (see Sect. 3).

Over the United States, the NADP measured nitrate deposition change between 1980 and 2000 consists mostly of reductions (by 50–100  $\text{mg(N) m}^{-2} \text{ yr}^{-1}$ , approximately 10–20 %), especially in the eastern portion of the United States (Fig. 3, top row). However, the MMM shows only a minor change over both the eastern and western United States. Indeed, all models except GISS (Table 6) indicate a relative increase in nitrate deposition averaged over the United States. This simulated increase in wet deposition is a combination of minor increases in  $\text{NO}_x$  emissions (Fig. S1a) and in precipitation amounts (Table 6). Based on the CPC Merged Analysis of Precipitation (CMAP; Xie and Arkin, 1997), there is however indication of a small observed decrease in precipitation between 1980 and 2000 over the United States (Fig. S2), while the MMM has limited inter-model agreement and actually shows a slight increase in precipitation when averaged over the whole United States (Table 6). It must however be recognized that the changes over the United States are relatively small and may therefore be strongly affected by interannual variability. Over the EMEP network, many sites indicate a very strong reduction consistent with emission change (Fig. S1a), with the exception of former Yugoslavia and the southern tip of Norway. The MMM captures well the strong reduction, with however a smaller amplitude than is observed at most locations. In this case (Table 6), all models agree on the change in emissions (-12 % for the mean) and all but MOCAGE show an increase in precipitation (1.6 % for the mean), the combination of both leading to an overall decrease in deposition (-9 % for the mean).

Measured ammonium deposition (Fig. 3, middle row) changes over the NADP network show a mixture of increases and decreases, with again the largest decreases over the Northeastern United States. Similar to nitrate deposition, the MMM is much more uniform than observed and only shows a small decrease in the mid-Western United States. This is due to the fact that the anthropogenic emissions of  $\text{NH}_3$  are almost identical between 1980 and 2000 (see Fig. S1b). This lack of change in emissions between 1980 and 2000 is possibly erroneous (either in the national total or in its regional distribution) but more analysis is beyond the scope of this paper. Over Europe, the EMEP station data indicate an overall strong decrease, with the exception of sites in France, Italy and Norway. The MMM indicates an overall small decrease

over Western Europe and a decrease over Eastern Europe, consistent with the significant emission change (Fig. S1b). Local factors, not included in the models, play a role in these differences.

Over the United States, except for a dozen sites scattered over the NADP network, observed sulfate deposition east of 100° W (Fig. 3, bottom row) is characterized by large reductions driven by emission change (Fig. S1c). The MMM is however underestimating the amplitude of the changes, especially for the largest changes. Over the EMEP network, the MMM captures well the general deposition decrease including its largest change over Germany (with values larger than 500 mg(S) m<sup>-2</sup> yr<sup>-1</sup>), clearly driven by the emission change (Fig. S1c).

Overall, the analysis of changes between 1980 and 2000 shows limited agreement between MMM and observations over the United States. In particular, the observed changes over the NADP network indicate much higher variability and amplitude than is simulated, driven by fairly small changes in emissions. Also, this analysis highlights the potential misrepresentation of the NH<sub>3</sub> emission change over the United States between 1980 and 2000. While the deposition change over Europe from the MMM is not as large as observed, the overall patterns of change are better represented, except for NH<sub>x</sub> deposition over Western Europe. This suggests that NO<sub>x</sub> (and to a lesser extent SO<sub>x</sub> and NH<sub>x</sub>) emissions changes may better captured over Europe in the historical emission dataset used in ACCMIP (Lamarque et al., 2010), since emission change is the main driver for deposition change. However, further analysis is required for a complete understanding of the applicability of deposition data to constrain emission inventories.

## 6 Evaluation of deposition changes: 1850–2000

In addition to recent surface measurements, we use ice core records of deposition over the Northern Hemisphere and Antarctica to study the ability of models to represent changes since 1850. To limit the importance of interannual variability in the ice-core record, we use the average values for 1850–1860 and 1995–2005 to compare against the 1850 and 2000 time slices, respectively. As a basic test of the applicability of the MMM to the polar regions, we show in Fig. S3 a comparison of year 2000 precipitation against the gauge-based climatology of Yang et al. (2005). We find that the MMM provides a regional distribution of precipitation consistent with the observations (including the annual amount) throughout the Arctic circle poleward of 60 N, with the caveat that no rain gauges are available over Central Greenland. Additional analysis of precipitation over the Arctic is provided in Lee et al. (2013). No equivalent data are available for Antarctica.

We find that there is a strong agreement between the 1850 observed and simulated nitrate depositions (Fig. 4a) for 1850, both in regional structure and intensity. Nitrate deposition in

2000 is however overestimated at all Northern Hemisphere sites but one. On the other hand, the year 2000 simulated deposition over Antarctica, which is much less affected by changes in anthropogenic NO<sub>x</sub> emissions but still shows an overall increase in nitrate deposition, is in good agreement with the observations.

Ammonium deposition (Fig. 4b) is strongly overestimated at the Greenland sites in both 1850 and 2000 time slices (and so is the change 2000 *minus* 1850; not shown). Wolff et al. (2013) argue that it is actually difficult to derive a change of measured NH<sub>4</sub><sup>+</sup> deposition over Greenland, due to the large dependency on the highly variable contribution of biomass burning to NH<sub>4</sub><sup>+</sup> deposition. On the other hand the other two sites in the Northern Hemisphere (McCall, Alaska and Akademii Nauk, Siberia; see Table S6 for their exact locations) are well captured. This is true for the 2000 time slice as well, where the McCall glacier shows a decrease since 1850, possibly associated with a change in biomass burning emissions over North America. Over Antarctica, ammonium deposition rates over the Eastern portion of the ice sheet are well represented, while they are somewhat overestimated in the Western sector. This is the case for both 1850 and 2000. Increases in the simulated deposition between 1850 and 2000 seem to be larger than observed, albeit the levels of deposition are small compared to those observed in the Northern Hemisphere.

Sulfate deposition in 1850 (Fig. 4c) is represented quite well at the Northern Hemisphere except for McCall, Alaska and central Greenland (Tunu glacier). Over Antarctica, the deposition tends to be slightly lower than observed, but with the accurate representation of the East-West gradient. Sulfate deposition in 2000 is overestimated at all ice-core sites of the Northern Hemisphere. Sulfate deposition over Antarctica has a well-defined east-west separation, well captured by the model. There is little variation between 1850 and 2000 since the sulfate production there is primarily driven by DMS oxidation. In many models used in ACCMIP, the DMS source does not vary with time, although Cameron-Smith et al. (2011) suggest it should, and changes in DMS emissions could represent an important feedback in the climate system (Charlson et al., 1987).

Overall, the ice-core comparison of the MMM indicates a reasonable representation of the pre-industrial (1850) conditions but tends to overestimate the present-day (2000) conditions. Similar conclusions are found for 1980 (not shown), indicating that biases in the year 2000 deposition fields are not related to recent transient features.

## 7 Total nitrogen and sulfate deposition 1850–2100

In this section, we document the MMM global and regional distributions of total deposition (wet + dry) of NO<sub>y</sub>, NH<sub>x</sub> and SO<sub>x</sub> and their changes from 1850 to 2100 under the RCP2.6, 4.5 and 8.5 projection scenarios (Fig. 5, Fig. S5

and Tables S2–S4; note that these tables also include regional emission totals).

The historical increase of  $\text{NO}_y$  deposition (Fig. 5a) since 1850 took place mostly in the Northern Hemisphere. It is characterized by deposition rates larger than  $100 \text{ mg(N) m}^{-2} \text{ yr}^{-1}$  over most of the continental areas, the North Atlantic and the outflow oceanic areas of Eastern Asia, the Indian subcontinent and Central Africa. By 2030, the projections over the United States and Europe are quite similar for RCP2.6 and RCP4.5, while RCP8.5 shows a smaller reduction from the 2000 levels. In Eastern Asia, deposition of  $\text{NO}_y$  is showing levels above 2000, with the largest increase seen in RCP8.5. On the other hand, over the Indian sub-continent the largest deposition increases were found in RCP4.5. Only small changes occur in the Southern Hemisphere. By 2100, most of the continental areas, except for India, are projected to return to pre-1980 levels of deposition. Another exception is the larger deposition over the Northern Pacific ocean in RCP8.5, consistent with increased  $\text{NO}_x$  emissions from shipping. Since the MMM  $\text{NO}_y$  deposition is computed from the largest number of models, it is reasonable to document intermodel variability for that diagnostic (Fig. S6). We find that over most continental areas and for most time slices, the inter-model standard deviation is in the 10–20 % range, with Central Asia and South America being somewhat larger (20–30 %). The higher standard deviation over South America stems from variations in soil emissions, while the variability over Central Asia is mostly related to precipitation differences (not shown).

While the increases in nitrogen deposition from ammonia emissions between 1850 and 2000 affect the various regions similarly to the impact of  $\text{NO}_x$  emissions (Fig. 5b), the RCP projections for  $\text{NH}_3$  emissions are indicative of a very different trajectory (Lamarque et al., 2011), with continuous increases over most regions, with the exception of the oceans south of  $30^\circ \text{ S}$ . These deposition changes are mainly driven by the projected increases in inorganic fertilizer use needed to provide more and higher quality food for a growing worldwide population, with no policies in places to abate the emissions.

Simulated sulfate deposition grew and was more widespread in Europe than North America in 1980, but was similar in both regions by 2000. The only significant increase between 1980 and 2000 is over China, associated with its increasing use of coal for power generation (Smith et al., 2011). The projected changes over these regions indicate a gradual phase-out of anthropogenic  $\text{SO}_2$  emissions by 2100, including over China. Even by 2030, emissions over China are projected to be no larger than in 2000, a trend that might be reflected in the most recent estimates over China (Smith et al., 2011; Klimont et al., 2013). Similar to  $\text{NO}_y$  deposition, only the Indian subcontinent is projected in RCP8.5 to have sulfate deposition levels higher in 2100 than in 1980. Sulfate deposition over the oceans is also considerably reduced in the

RCP scenarios, but depends on the specific scenario's projection of shipping emissions.

The combination of deposition fluxes as  $2 \cdot \text{SO}_x + \text{NO}_y - \text{NH}_x$  provides an indication of the degree of additional acidity (Keene et al., 1983) contained in the deposited fluxes from the emissions of the precursor compounds (Fig. 6). In particular, it shows that, over the 21st century, continental areas over the Northern Hemisphere will have a tendency towards more basic deposition with the increase  $\text{NH}_3$  emissions. This analysis also clearly shows the spurious  $\text{NH}_3$  emissions over Mongolia (as discussed in Sect. 4).

Following the discussion of averaged deposition rates over various regions in Lamarque et al. (2011 see their Tables 5 and 6; note that the NCAR-CAM3.5 results used in the present ACCMIP analysis are equivalent to results in the present analysis), we present the same diagnostics here (in the same units), with the exception of RCP6.0 (Tables 7 and 8). Overall, the total (from  $\text{NO}_y$  and  $\text{NH}_x$  combined, since both affect vegetation in the same fashion) nitrogen deposition is expected to increase between 2000 and 2100 over many regions, especially in the case of RCP8.5. Furthermore, only Western Europe and North America are projected to see a reduction in their nitrogen deposition. Sulfate deposition rates are clearly projected to significantly decrease by 2100, as expected from Fig. 5. All these confirm the results published in Lamarque et al. (2011) in a single model study using the same emission fields applied in the present study.

## 8 Discussion and conclusions

We have presented in this paper the multi-model mean annual deposition fields of nitrogen and sulfate as simulated in the Atmospheric Chemistry and Climate Model Intercomparison Project (Lamarque et al., 2013). We have made considerable use of network-based wet deposition datasets (including a new dataset based on expert analysis of the deposition data; Vet et al., 2013) and found that the ACCMIP multi-model mean performs similarly (in terms of mean bias and correlation coefficient for the annual mean) to previous multi-model analysis (Dentener et al., 2006; Sanderson et al., 2008), with the notable exception of ammonium deposition over Asia, which is considerably worse in ACCMIP due to a regridding error in the underlying emissions over the China-Mongolia region (Lamarque et al., 2010).

Beyond the present-day analysis, we discuss a comparison of the change in deposition rates between 1980 and 2000 (using surface wet deposition) and between 1850 and 2000 (using ice-cores). Although the deposition in 2000 is rather well simulated in ACCMIP, there are considerable differences between the estimated change from 1980 to 2000 and the simulated one. This is particularly the case over the United States, where changes in anthropogenic  $\text{NH}_x$  (and to a lesser extent  $\text{NO}_x$ ) emissions are much smaller than over Europe, and do

not lead to the observed deposition rate changes. In terms of ice-core analysis, the ACCMIP multi-model mean captures many of the regional features of deposition, but there seems to be an overall overestimation of nitrogen deposition in 2000 over the Arctic, while Antarctic deposition fluxes are well simulated.

The discussion of the total deposition (wet + dry) in the ACCMIP multi-model mean confirms to a large extent the single-model results discussed in Lamarque et al. (2011). In particular, there are large regional increases in 2100 N deposition in Latin America, Africa and parts of Asia under some of the scenarios considered. Increases in South Asia are especially large, and are seen in all scenarios, with 2100 values more than double 2000 in some scenarios and reaching region averaged values of  $> 1300 \text{ mg(N) m}^{-2} \text{ yr}^{-1}$  in RCP 2.6 and 8.5,  $\sim 30\text{--}50\%$  larger than the values in any region currently (*circa* 2000). On the other hand, no regions with sulfur deposition fields in 2100 larger than 2000 are identified. The multi-model mean deposition fields as discussed in this study are available at [http://acd.ucar.edu/~lamar/ACCMIP/Deposition/all\\_fields\\_062013.tar.gz](http://acd.ucar.edu/~lamar/ACCMIP/Deposition/all_fields_062013.tar.gz).

Numerical experiments such as described in the present paper highlight regions of deposition where routine measurements are unavailable. For example, few measurements are available in South America or Africa where the projected RCP changes between 2000 and 2100 are significant increases, according the RCP projections used here. On the other hand, it is clear that the expansion of measurement capabilities highlight the necessity for a better and higher resolution representation of emissions. Finally, the analysis presented here shows that there is strong potential in using nitrogen and sulfate deposition observational data to identify gaps in our understanding (and possibly constrain) the change in respective precursor emissions. Expansion of the WMO wet deposition assessment to earlier periods and more ice cores (especially in the vicinity of polluted areas, such as the Alps or Himalayas) can provide a window on nitrogen and sulfate emission changes, possibly helping to understand the inability of current models to reproduce the observed long-term trends in Northern Hemisphere surface ozone (Lamarque et al., 2010).

**Supplementary material related to this article is available online at:** <http://\@journalurl/\@pvol/\@fpage/\@pyear/\@journalnameshortlower-\@pvol-\@fpage-\@pyear-supplement.pdf>.

*Acknowledgement.* ACCMIP is organized under the auspices of Atmospheric Chemistry and Climate AC&C, a project of International Global Atmospheric Chemistry (IGAC) and Stratospheric Processes And their Role in Climate (SPARC) under the International Geosphere-Biosphere Project (IGBP) and World Climate Research Program (WCRP). The authors are grateful to the British

Atmospheric Data Centre (BADC), which is part of the NERC National Centre for Atmospheric Science (NCAS), for collecting and archiving the ACCMIP data. D. S., G. F. and Y. L. acknowledge support from the NASA MAP and ACMAP programs. D. P. would like to thank the Canadian Foundation for Climate and Atmospheric Sciences for their long-running support of CMAM development. S. G. was supported by the US Department of Energy Office of Science Decadal and Regional Climate Prediction using Earth System Models (EaSM) program. The Pacific Northwest National Laboratory (PNNL) is operated for the DOE by Battelle Memorial Institute under contract DE-AC06-76RLO 1830. The work of D. B. and P. C.-S. was funded by the US Dept. of Energy (BER), performed under the auspices of LLNL under Contract DE-AC52-07NA27344, and used the supercomputing resources of NERSC under contract No. DE-AC02-05CH11231. G. Z. acknowledges NIWA HPCF facility and funding from New Zealand Ministry of Science and Innovation. The GEOSCCM work was supported by the NASA Modeling, Analysis and Prediction program, with computing resources provided by NASA's High-End Computing Program through the NASA Advanced Supercomputing Division. The STOC-HadAM3 work made use of the facilities of HECToR, the UK national high-performance computing service which is funded by the Office of Science and Technology through EPSRC High End Computing Programme. The CICERO-OsloCTM2 simulations were done within the projects SLAC (Short Lived Atmospheric Components) and EarthClim funded by the Norwegian Research Council and ECLIPSE (Evaluating the Climate and Air Quality Impacts of Short-Lived Pollutants) funded by the European Union. The MOCAGE simulations were supported by Météo-France and CNRS. Supercomputing time was provided by Météo-France/DSI supercomputing center. The CESM project (which includes CESM-CAM-Superfast, NCAR-CAM3.5 and NCAR-CAM5.1) is supported by the National Science Foundation and the Office of Science (BER) of the US Department of Energy. The National Center for Atmospheric Research is operated by the University Corporation for Atmospheric Research under sponsorship of the National Science Foundation. CMAP Precipitation data are provided by the NOAA/OAR/ESRL PSD, Boulder, Colorado, USA, from their Web site at <http://www.esrl.noaa.gov/psd/>. We thank Robert Vet and his precipitation chemistry assessment team, to make the WMO deposition dataset available prior to publication. We acknowledge the substantial efforts of the field and logistics personnel involved in collecting the ice cores including those from WAIS Divide, the Norwegian-United States Scientific Traverse of East Antarctica, and NEEM. We also thank Dan Pasteris and the other students and staff of the DRI ultra-trace ice core chemistry laboratory for help in analyzing the ice cores and the Office of Polar Programs at the National Science Foundation for supporting collection and analysis of the cores.

## References

- Andres, R. J. and Kasgnoc, A. D.: A time-averaged inventory of subaerial volcanic sulfur emissions, *J. Geophys. Res.*, 103, 25251–25261, doi:<http://dx.doi.org/10.1029/98JD020911>, 1998.
- Anschütz, H., Sinisalo, A., Isaksson, E., McConnell, J. R., Hamran, S.-E., Bisiaux, M. M., Pasteris, D., Neumann, T. A., and Winther, J.-G.: Variation of accumulation rates over the last

- eight centuries on the East Antarctic Plateau derived from volcanic signals in ice cores, *J. Geophys. Res.*, 116, D20103, doi:<http://dx.doi.org/10.1029/2011JD015753>, 2011.
- Boucher, O., Moulin, C., Belviso, S., Aumont, O., Bopp, L., Cosme, E., von Kuhlmann, R., Lawrence, M. G., Pham, M., Reddy, M. S., Sciare, J., and Venkataraman, C.: DMS atmospheric concentrations and sulphate aerosol indirect radiative forcing: a sensitivity study to the DMS source representation and oxidation, *Atmos. Chem. Phys.*, 3, 49–65, doi:<http://dx.doi.org/10.5194/acp-3-49-2003>, 2003.
- Bobbink, R., Hicks, K., Galloway, J., Spranger, T., Alkemade, R., Ashmore, M., Bustamante, M., Cinderby, S., Davidson, E., Dentener, F., Emmett, B., Erisman, J. W., Fenn, M., Gilliam, F., Nordin, A., Pardo, L., and de Vries, W.: Nitrogen deposition and plant diversity, *Ecol. Appl.*, 20, 30–59, 2010.
- Bouwman, A. F., Van Vuuren, D. P., Derwent, R. G., and Posch, M.: A global analysis of acidification and eutrophication of terrestrial ecosystems, *Water Air Soil Pollut.*, 141, 349–382, doi:<http://dx.doi.org/10.1023/A:102139800872610>, 2002.
- Butchart, S. H. M., Walpole, M., Collen, B., van Strien, A., Scharlemann, J. P. W., Almond, R. E. A., Baillie, J. E. M., Bomhard, B., Brown, C., Bruno, J., Carpenter, K. E., Carr, G. M., Chanson, J., Chenery, A. M., Csirke, J., Davidson, N. C., Dentener, F., Foster, M., Galli, A., Galloway, J. N., Genovesi, P., Gregory, R. D., Hockings, M., Kapos, V., Lamarque, J. F., Leverington, F., Loh, J., McGeoch, M. A., McRae, L., Minasyan, A., Hernández Morcillo, M., Oldfield, T. E. E., Pauly, D., Quader, S., Revenga, C., Sauer, J. R., Skolnik, B., Spear, D., Stanwell-Smith, D., Stuart, S. N., Symes, A., Tierney, M., Tyrrell, T. D., Vié, J., and Watson, R.: Global biodiversity: indicators of recent declines, *Science*, 328, 1164, doi:<http://dx.doi.org/10.1126/science.1187512>, 2010.
- Cameron-Smith, P., Elliott, S., Maltrud, M., Erickson, D., and Wingenter, O.: Changes in dimethyl sulfide oceanic distribution due to climate change, *Geophys. Res. Lett.*, 38, L07704, doi:<http://dx.doi.org/10.1029/2011GL047069>, 2011.
- Charlson, R. J., Lovelock, J. E., Andreae, M. O., and Warren, S. G.: Oceanic phytoplankton, atmospheric sulphur, cloud albedo, and climate, *Nature*, 326, 655–665, doi:<http://dx.doi.org/10.1038/326655a0>, 1987.
- Dentener, F., Drevet, J., Lamarque, J. F., Bey, I., Eickhout, B., Fiore, A. M., Hauglustaine, D., Horowitz, L. W., Krol, M., Kulshrestha, U. C., Lawrence, M., Galy-Lacaux, C., Rast, S., Shindell, D., Stevenson, D., Van Noije, T., Atherton, C., Bell, N., Bergman, D., Butler, T., Cofala, J., Collins, B., Doherty, R., Ellingsen, K., Galloway, J., Gauss, M., Montanaro, V., Müller, J. F., Pitari, G., Rodriguez, J., Sanderson, M., Solomon, F., Strahan, S., Schultz, M., Sudo, K., Szopa, S., and Wild, O.: Nitrogen and sulfur deposition on regional and global scales: a multimodel evaluation, *Global Biogeochem. Cy.*, 20, GB4003, doi:<http://dx.doi.org/10.1029/2005GB002672>, 2006.
- Fisher, J. A., Jacob, D. J., Wang, Q., Bahreini, R., Carouge, C. C., Cubison, M. J., Dibb, J. E., Diehl, T., Jimenez, J. L., Leibensperger, E. M., Lu, Z., Meinders, M. B. J., Pye, H. O. T., Quinn, P. K., Sharma, S., Streets, D. G., van Donkelaar, A., and Yantosca, R. M.: Sources, distribution, and acidity of sulfate-ammonium aerosol in the Arctic in winter-spring, *Atmos. Environ.*, 45, 7301–7318, 2011.
- Fowler, D., Coyle, M., Skiba, U., Sutton, M., Cape, N., Reiss, S., Sheppard, L., Jenkins, A., Galloway, J., Vitousek, P., Leech, A., Bouwman, L., Butterbach-Bahl, K., Dentener, F., Stevenson, D., Amann, M., and Voss, M.: The global nitrogen cycle in the 21st century, submitted to *Philos. T. Roy. Soc. Ser. B*, 2012.
- Galloway, J. N., Townsend, A. R., Erisman, J. W., Bekund, M., Cai, Z., Freney, J. R., Martinelli, L. A., Seitzinger, S. P., and Sutton, M. A.: Transformation of the nitrogen cycle: recent trends, questions and potential solutions, *Science*, 320, 889–889, 2008.
- Granier, C., Bessagnet, B., Bond, T., D'Angiola, A., Denier van der Gon, H., Frost, G., Heil, A., Kaiser, J., Kinne, S., Klimont, Z., Kloster, S., Lamarque, J.-F., Lioussé, C., Masui, T., Meleux, F., Mieville, A., Ohara, T., Raut, J.-C., Riahi, K., Schultz, M., Smith, S., Thompson, A., van Aardenne, J., van der Werf, G., and van Vuuren, D.: Evolution of anthropogenic and biomass burning emissions of air pollutants at global and regional scales during the 1980–2010 period, *Clim. Change*, 109, 163–190, 2011.
- Kanakidou, M., Duce, R. A., Prospero, J. M., Baker, A. R., Benitez-Nelson, C., Dentener, F. J., Hunter, K. A., Liss, P. S., Mahowald, N., Okin, G. S., Sarin, M., Tsigaridis, K., Uematsu, M., Zamora, L. M., and Zhu, T.: Atmospheric fluxes of organic N and P to the global ocean, *Global Biogeochem. Cy.*, 26, GB3026, doi:<http://dx.doi.org/10.1029/2011GB004277>, 2012.
- Keene, W. C., Galloway, J. N. and Holden, J. D.: Measurement of weak organic acidity in precipitation from remote areas of the world, *J. Geophys. Res.*, 88, 5122–5130, 1983.
- Klimont, Z., Smith, S. J., and Cofala, J.: The last decade of global anthropogenic sulfur dioxide: 2000–2011 emissions, *Environ. Res. Lett.*, 8, 014003, doi:<http://dx.doi.org/10.1088/1748-9326/8/1/014003>, 2013.
- Lamarque, J. F., Kiehl, J. T., Brasseur, G. P., Butler, T., Cameron-Smith, P., Collins, W. D., Collins, W. J., Granier, C., Hauglustaine, D., Hess, P. G., Holland, E. A., Horowitz, L., Lawrence, M. G., McKenna, D., Merilees, P., Prather, M. J., Rasch, P. J., Rotman, D., Shindell, D., and Thornton, P.: Assessing future nitrogen deposition and carbon cycle feedback using a multimodel approach: analysis of nitrogen deposition, *J. Geophys. Res.*, 110, D19303, doi:<http://dx.doi.org/10.1029/2005JD005825>, 2005.
- Lamarque, J.-F., Bond, T. C., Eyring, V., Granier, C., Heil, A., Klimont, Z., Lee, D., Lioussé, C., Mieville, A., Owen, B., Schultz, M. G., Shindell, D., Smith, S. J., Stehfest, E., Van Aardenne, J., Cooper, O. R., Kainuma, M., Mahowald, N., McConnell, J. R., Naik, V., Riahi, K., and van Vuuren, D. P.: Historical (1850–2000) gridded anthropogenic and biomass burning emissions of reactive gases and aerosols: methodology and application, *Atmos. Chem. Phys.*, 10, 7017–7039, doi:<http://dx.doi.org/10.5194/acp-10-7017-2010>, 2010.

- Lamarque, J.-F., Kyle, G. P., Meinshausen, M., Riahi, K., Smith, S. J., van Vuuren, D. P., Conley, A., and Vitt, F.: Global and regional evolution of short-lived radiatively-active gases and aerosols in the Representative Concentration Pathways, *Clim. Change*, doi:<http://dx.doi.org/10.1007/s10584-011-0155-0>, 2011.
- Lamarque, J.-F., Shindell, D. T., Josse, B., Young, P. J., Cionni, I., Eyring, V., Bergmann, D., Cameron-Smith, P., Collins, W. J., Doherty, R., Dalsoren, S., Faluvegi, G., Folberth, G., Ghan, S. J., Horowitz, L. W., Lee, Y. H., MacKenzie, I. A., Nagashima, T., Naik, V., Plummer, D., Righi, M., Rumbold, S. T., Schulz, M., Skeie, R. B., Stevenson, D. S., Strode, S., Sudo, K., Szopa, S., Voulgarakis, A., and Zeng, G.: The Atmospheric Chemistry and Climate Model Intercomparison Project (ACCMIP): overview and description of models, simulations and climate diagnostics, *Geosci. Model Dev.*, 6, 179–206, doi:<http://dx.doi.org/10.5194/gmd-6-179-2013>, 2013.
- Lee, Y. H., Lamarque, J.-F., Flanner, M. G., Jiao, C., Shindell, D. T., Berntsen, T., Bisiaux, M. M., Cao, J., Collins, W. J., Curran, M., Edwards, R., Faluvegi, G., Ghan, S., Horowitz, L. W., McConnell, J. R., Myhre, G., Nagashima, T., Naik, V., Rumbold, S. T., Skeie, R. B., Sudo, K., Takemura, T., and Thevenon, F.: Evaluation of preindustrial to present-day black carbon and its albedo forcing from ACCMIP (Atmospheric Chemistry and Climate Model Intercomparison Project), *Atmos. Chem. Phys.*, 13, 2607–2634, doi:<http://dx.doi.org/10.5194/acp-13-2607-2013>, 2013.
- Masui, T., Matsumoto, K., Hijioka, Y., Kinoshita, T., Nozawa, T., Ishiwatari, S., Kato, E., Shukla, P. R., Yamagata, Y., and Kainuma, M.: An emission pathway for stabilization at  $6\text{ W m}^{-2}$  radiative forcing, *Clim. Change*, 109, 59–76, doi:<http://dx.doi.org/10.1007/s10584-011-0150-5>, 2011.
- McConnell, J. R. and Edwards, R.: Coal burning leaves toxic heavy metal legacy in the Arctic, *Proc. Natl. Acad. Sci. USA*, 105, 12140–12144, doi:<http://dx.doi.org/10.1073/pnas.0803564105>, 2008.
- Moss, R. H., Edmonds, J. A., Hibbard, K. A., Manning, M. R., Rose, S. K., van Vuuren, D. P., Carter, T. R., Emori, S., Kainuma, M., Kram, T., Meehl, G. A., Mitchell, J. F. B., Nakicenovic, N., Riahi, K., Smith, S. J., Stouffer, R. J., Thomson, A. M., Weyant, J. P., and Wilbanks, T. J.: The next generation of scenarios for climate change research and assessment, *Nature*, 463, 747–756, doi:<http://dx.doi.org/10.1038/nature08823>, 2010.
- Murphy, D. and Fahey, D.: An estimate of the flux of stratospheric reactive nitrogen and ozone into the troposphere, *J. Geophys. Res.*, 99, 5325–5332, doi:<http://dx.doi.org/10.1029/93JD03558>, 1994.
- Opel, T., Fritzsche, D., Meyer, H., Schuett, R., Weiler, K., Ruth, U., Wilhelms, F., and Fischer, H.: 115 year ice core record from Akademii Nauk ice cap, Severnaya Zemlya: high-resolution record of Euroasian Arctic climate change, *J. Glaciol.*, 55, 21–31, 2009.
- Phoenix, G. K., Hicks, W. K., Cinderby, S., Kuylenstierna, J. C. I., Stock, W. D., Dentener, F. J., Giller, K. E., Austin, A. T., Lefroy, R. D. B., Gimeno, B. S., Ashmore, M. R., and Ineson, P.: Atmospheric nitrogen deposition in world biodiversity hotspots: the need for a greater global perspective in assessing N deposition impacts, *Glob. Change Biol.*, 12, 470–476, doi:<http://dx.doi.org/10.1111/j.1365-2486.2006.01104.x>, 2006.
- Prather, M. J., Holmes, C. D., and Hsu, J.: Reactive greenhouse gas scenarios: systematic exploration of uncertainties and the role of atmospheric chemistry, *Geophys. Res. Lett.*, 39, L09803, doi:<http://dx.doi.org/10.1029/2012GL051440>, 2012.
- Reay, D. S., Dentener, F., Smit, P., Grace, J., and Feely, R. A.: Global nitrogen deposition and carbon sinks, *Nature Geosci.*, 1, 430–437, doi:<http://dx.doi.org/10.1038/ngeo230>, 2008.
- Reichler, T. and Kim, J.: How well do coupled models simulate today's climate?, *B. Am. Meteorol. Soc.*, 89, 303–311, 2008.
- Rodhe, H., Dentener, F., and Schulz, M.: The global distribution of acidifying wet deposition, *Environ. Sci. Tech.*, 36, 4382–4388, 2002.
- Roethlisberger, R., Bigler, M., Hutterli, M., Sommer, S., Stauffer, B., Junghans, H. G., and Wagenbach, D.: Technique for continuous high-resolution analysis of trace substances in firn and ice cores, *Environ. Sci. Technol.*, 34, 338–342, 606–607, 2000.
- Sanderson, M. G., Dentener, F. J., Fiore, A. M., Cuvelier, C., Keating, T. J., Zuber, A., Atherton, C. S., Bergmann, D. J., Diehl, T., Doherty, R. M., Duncan, B. N., Hess, P., Horowitz, L. W., Jacob, D., Jonson, J.-E., Kaminski, J. W., Lupu, A., Mackenzie, I. A., Marmer, E., Montanaro, V., Park, R., Pitari, G., Prather, M. J., Pringle, K. J., Schroeder, S., Schultz, M. G., Shindell, D. T., Szopa, S., Wild, O., and Wind, P.: A multi-model source-receptor study of the hemispheric transport and deposition of oxidised nitrogen, *Geophys. Res. Lett.*, 35, L17815, doi:<http://dx.doi.org/10.1029/2008GL035389>, 2008.
- Singh, Y., and Berninger, F.: Sulphur deposition causes a large-scale growth decline in boreal forests in Eurasia, *Global Biogeochem. Cycles*, 24, GB3002, doi:<http://dx.doi.org/10.1029/2009GB003749>, 2008.
- Shindell, D. T., Lamarque, J. F., Schulz, M., Flanner, M., Jiao, C., Chin, M., Young, P., Lee, Y. H., Rotstayn, L., Milly, G., Faluvegi, G., Balkanski, Y., Collins, W. J., Conley, A. J., Dalsoren, S., Easter, R., Ghan, S., Horowitz, L., Liu, X., Myhre, G., Nagashima, T., Naik, V., Rumbold, S., Skeie, R., Sudo, K., Szopa, S., Takemura, T., Voulgarakis, A., and Yoon, J.-H.: Radiative forcing in the ACCMIP historical and future climate simulations, *Atmos. Chem. Phys.*, 13, 2939–2974, doi:<http://dx.doi.org/10.5194/acp-13-2939-2013>, 2013.
- Sigl, M., McConnell, J. R., Layman, L., Maselli, O., McGwire, K., Pasteris, D., Dahl-Jensen, D., Steffensen, J. P., Edwards, R., and Mulveney, R.: A new bipolar ice core record of volcanism from WAIS Divide and NEEM and implications for climate forcing of the last 2000 years, *J. Geophys. Res.*, 118, 3, 1151–1169, doi:<http://dx.doi.org/10.1029/2012JD018603>, 2013.

- Smith, S. J., van Aardenne, J., Klimont, Z., Andres, R. J., Volke, A., and Delgado Arias, S.: Anthropogenic sulfur dioxide emissions: 1850–2005, *Atmos. Chem. Phys.*, 11, 1101–1116, doi:<http://dx.doi.org/10.5194/acp-11-1101-2011>, 2011.
- Sutton, M. A., Oenema, O. Erisman, J. W., Leip, A., van Grinsven, H., and Winiwarter, W.: Too much of a good thing, *Nature*, 472, 159–161, 2011.
- Taylor, K. E., Stouffer, R. J., and Meehl, G. A.: An overview of CMIP5 and the experiment design, *B. Am. Meteorol. Soc.*, 93, 485–498, 2012.
- Thornton, P. E., Doney, S. C., Lindsay, K., Moore, J. K., Mahowald, N., Randerson, J. T., Fung, I., Lamarque, J.-F., Fedema, J. J., and Lee, Y.-H.: Carbon-nitrogen interactions regulate climate-carbon cycle feedbacks: results from an atmosphere-ocean general circulation model, *Biogeosciences*, 6, 2099–2120, doi:<http://dx.doi.org/10.5194/bg-6-2099-2009>, 2009.
- van Aardenne, J. A., Dentener, F. J., Klijn Goldewijk, C. G. M., Lelieveld, J., and Olivier, J. G. J.: A  $1^\circ - 1^\circ$  resolution dataset of historical anthropogenic trace gas emissions for the period 1890–1990, *Global Biogeochem. Cy.*, 15, 909–928, 2001.
- van Vuuren, D. P., Edmonds, J., Kainuma, M., Riahi, K., Thomson, A., Hibbard, K., Hurtt, G. C., Kram, T., Krey, V., Lamarque, J.-F., Matsui, T., Meinshausen, M., Nakicenovic, N., Smith, S. J., and Rose, S. K.: The representative concentration pathways: an overview, *Clim. Change*, 109, 5–31, doi:<http://dx.doi.org/10.1007/s10584-011-0148-z>, 2011.
- Vet R., Artz, R., Shaw, M., Ro, C.-U., Carou, S., Aas, W., Baker, A., Bowersox, V., Dentener, F., Galy-Lacaux, C., Hou, A., Pienaar, K., Gillett, R., Forti, M. C., Gromov S., Hara, H., Khodzher, T., Mahowald, N., Nickovic, N., Rao, P. S. P., and Reid, N.: A global assessment of precipitation chemistry and deposition, submitted to *Atmospheric Environment*, 2013.
- Wolff, E. W.: Ice sheets and nitrogen, *Philos. Trans. R. Soc. Ser. B*, 368, doi:<http://dx.doi.org/10.1098/rtsb.2013.0127>, 2013.
- WMO/GAW, 2004. Manual for the GAW Precipitation Chemistry Programme: Guidelines, Data Quality Objectives and Standard Operating Procedures. World Meteorological Organization/Global Atmosphere Watch, No. 160. Geneva, Switzerland.
- Xie, P. and Arkin, P. A.: Global precipitation: A 17-year monthly analysis based on gauge observations, satellite estimates, and numerical model outputs, *B. Am. Meteorol. Soc.*, 78, 2539–2558, 1997.
- Xing, J., Pleim, J., Mathur, R., Pouliot, G., Hogrefe, C., Gan, C.-M., and Wei, C.: Historical gaseous and primary aerosol emissions in the United States from 1990–2010, *Atmos. Chem. Phys. Discuss.*, 12, 30327–30369, doi:<http://dx.doi.org/10.5194/acpd-12-30327-2012>, 2012.
- Yang, D., Kane, D., Zhang, Z. Legates, D., and Goodison, B.: Bias-corrections of long-term (1973–2004) daily precipitation data over the northern regions, *Geophys. Res. Lett.*, 32, L19501, doi:<http://dx.doi.org/10.1029/2005GL024057>, 2005.
- Young, P. J., Archibald, A. T., Bowman, K. W., Lamarque, J.-F., Naik, V., Stevenson, D. S., Tilmes, S., Voulgarakis, A., Wild, O., Bergmann, D., Cameron-Smith, P., Cionni, I., Collins, W. J., Dalsøren, S. B., Doherty, R. M., Eyring, V., Faluvegi, G., Horowitz, L. W., Josse, B., Lee, Y. H., MacKenzie, I. A., Nagashima, T., Plummer, D. A., Righi, M., Rumbold, S. T., Skeie, R. B., Shindell, D. T., Strode, S. A., Sudo, K., Szopa, S., and Zeng, G.: Pre-industrial to end 21st century projections of tropospheric ozone from the Atmospheric Chemistry and Climate Model Intercomparison Project (ACCMIP), *Atmos. Chem. Phys.*, 13, 2063–2090, doi:<http://dx.doi.org/10.5194/acp-13-2063-2013>, 2013.
- Zachle, S., Friedlingstein, P., and Friend, A. D. Terrestrial nitrogen feedbacks may accelerate future climate change, *Geophys. Res. Lett.*, 37, L01401, doi:<http://dx.doi.org/10.1029/2009GL041345>, 2010.
- Zhang, L., Jacob, D. J., Knipping, E. M., Kumar, N., Munger, J. W., Carouge, C. C., van Donkelaar, A., Wang, Y. X., and Chen, D.: Nitrogen deposition to the United States: distribution, sources, and processes, *Atmos. Chem. Phys.*, 12, 4539–4554, doi:<http://dx.doi.org/10.5194/acp-12-4539-2012>, 2012.

**Table 1.** List and principal characteristics of ACCMIP simulations (P indicates the primary simulations, O the optional ones). SSTs stands for sea-surface temperatures and GHGs for greenhouse gases. Adapted from Lamarque et al. (2013).

Historical simulations	1850	1930	1980	2000
Emissions and SSTs/GHG for given year	P	P	P	P
Future simulations	2010	2030	2050	2100
RCP 2.6 (emissions, GHGs and SSTs)		P	O	P
RCP 4.5 (emissions, GHGs and SSTs)	O	O	O	O
RCP 6.0 (emissions, GHGs and SSTs)	P	P	O	P
RCP 8.5 (emissions, GHGs and SSTs)		P	O	P

**Table 2.** Summary of global totals ( $\text{Tg(N) yr}^{-1}$ ) for deposition and emissions in 2000 related to the nitrogen oxide emissions. Total dep. (4th column) is the sum of wet and dry deposition while Total emi. (7th column) is the sum of  $\text{NO}_x$  surface and aircraft emissions (eminox) and lightning emissions (emilnox). Note that deposition is equal or slightly larger than emissions due to the net input of nitrogen (usually in the form of nitric acid) from the stratosphere (approx.  $1 \text{ Tg(N) yr}^{-1}$ , except for the GISS models which have a  $5 \text{ Tg(N) yr}^{-1}$  input from the stratosphere). All numbers are rounded to the nearest integer.

Model	Dry	Wet	Total dep.	eminox	emilnox $\text{Tg(N) yr}^{-1}$	Total emi.
CESM-CAM-superfast	17	29	46	42	4	46
CICERO-OsloCTM2	31	24	54			52
CMAM	27	23	50	47	4	51
GEOSCCM	12	33	45	40	5	45
GISS-E2-R	14	39	53	41	8	49
GISS-E2-TOMAS	17	37	54	41	8	49
MOCAGE	20	27	47	43	5	48
NCAR-CAM3.5	20	29	49	43	4	47
STOC-HadAM3	26	27	52	45	7	52
UM-CAM	31	26	56	49	5	54
Multi-model mean	21	29	51	47	6	49
PhotoComp			51			

**Table 3.** Summary of global totals ( $\text{Tg(N) yr}^{-1}$ ) for year 2000 of deposition and emissions related to the ammonia emissions. Total (6th column) is the sum of wet and dry deposition for  $\text{NH}_3$  and  $\text{NH}_4$ . Eminh3 includes anthropogenic and natural (soils and oceans) emissions. All numbers are rounded to the nearest integer.

Model	Dry $\text{NH}_3$	Wet $\text{NH}_3$	Dry $\text{NH}_4^+$ $\text{Tg(N) yr}^{-1}$	Wet $\text{NH}_4^+$	Total	eminh3
CICERO-OsloCTM2	12	9	4	25	50	51
GISS-E2-R	22	5	4	29	58	57
GISS-E2-TOMAS	11	1	7	42	59	59
NCAR-CAM3.5	14	16	7	24	60	59
STOC-HadAM3	29	8	6	19	61	62
Multi-model mean	18	8	6	28	57	58
PhotoComp					64	

**Table 4.** Summary of global totals ( $\text{Tg(S)yr}^{-1}$ ) for year 2000 of deposition and emissions related to the sulfur emissions. Total dep. (4th column) is the sum of wet and dry deposition (both sums of  $\text{SO}_2$  and  $\text{SO}_4^{2-}$ ) while Total emi. (8th column) is the sum of  $\text{SO}_2$ ,  $\text{SO}_4^{2-}$  and DMS emissions. Note that the deposition total should be smaller than emission total since the formation of sulfate from the oxidation of DMS has a yield smaller than 1; this was estimated to be 87 % in Boucher et al. (2003) when both gas-phase and aqueous-phase reactions are taken into account. All numbers are rounded to the nearest integer.

Model	Dry	Wet	Total dep.	emiso2	emiso4	emidms	Total emi.
$\text{Tg(S)yr}^{-1}$							
CESM-CAM-superfast	36	45	81	64	0	19	83
CICERO-OsloCTM2	32	63	95	65	1	29	96
GISS-E2-R	51	45	95	65	2	28	95
GISS-E2-TOMAS	47	44	91	65	2	28	94
NCAR-CAM3.5	24	55	79	64	0	19	83
NCAR-CAM5.1	25	56	81	65	1	18	84
STOC-HadAM3	41	43	84	69	0	20	89
Multi-model mean	37	50	87	65	1	23	89
PhotoComp			80				

**Table 5.** Summary of statistical analysis of the evaluation of nitrate wet deposition (wetno3), ammonium wet deposition (wetnh4) and sulfate wet deposition (wetso4) for PhotoComp, HTAP and ACCMIP MMM over the 3 main analysis regions. Mean bias (model *minus* observations), observations and model are in  $\text{mg(N or S)/m}^2/\text{year}$ .

	North America			wetno3 Europe			Asia		
	PhotoComp	HTAP	ACCMIP	PhotoComp	HTAP	ACCMIP	PhotoComp	HTAP	ACCMIP
Linear fit slope	1.0	1.0	0.9	0.3	0.3	0.3	0.5	0.5	0.4
Linear fit intercept	1.0	1.0	0.9	0.3	0.3	0.3	0.5	0.5	0.4
Mean bias	34.8	21.9	44.3	-41.4	-60.0	-75.2	-47.8	-49.3	-46.4
Mean observations	191.3	191.3	191.3	300.5	300.5	300.5	263.0	263.0	263.0
Mean model	226.1	213.3	235.6	259.1	240.5	225.3	215.2	213.7	216.7
Correlation coefficient	0.8	0.9	0.9	0.6	0.6	0.6	0.8	0.8	0.8
Fraction within $\pm 50\%$	77.0	84.3	68.7	75.0	85.2	85.2	84.0	84.0	88.0

	North America			wetnh4 Europe			Asia		
	PhotoComp	HTAP	ACCMIP	PhotoComp	HTAP	ACCMIP	PhotoComp	HTAP	ACCMIP
Linear fit slope	0.8	0.9	0.5	0.4	0.4	0.3	0.8	0.7	0.1
Linear fit intercept	0.8	0.9	0.5	0.4	0.4	0.3	0.8	0.7	0.1
Mean bias	5.5	10.9	-12.1	-23.9	-49.7	-94.7	-69.7	-63.4	-136.2
Mean observations	161.3	161.3	161.3	336.0	336.0	336.0	400.5	400.5	400.5
Mean model	166.8	172.2	149.2	312.1	286.4	241.3	330.8	337.1	264.4
Correlation coefficient	0.9	0.9	0.8	0.6	0.6	0.6	0.8	0.8	0.2
Fraction within $\pm 50\%$	82.2	84.8	75.7	73.9	79.5	78.4	76.0	68.0	56.0

	North America			wetso4 Europe			Asia		
	PhotoComp	HTAP	ACCMIP	PhotoComp	HTAP	ACCMIP	PhotoComp	HTAP	ACCMIP
Linear fit slope	0.9	1.0	0.6	0.4	0.6	0.3	0.4	0.5	0.3
Linear fit intercept	0.9	1.0	0.6	0.4	0.6	0.3	0.4	0.5	0.3
Mean bias	46.3	50.0	-18.8	-67.2	51.5	-125.3	-218.6	-182.1	-292.4
Mean observations	309.8	309.8	309.8	404.5	404.5	404.5	686.1	686.1	686.1
Mean model	356.1	359.8	291.0	337.3	456.1	279.3	467.5	504.1	393.7
Correlation coefficient	0.9	0.9	0.9	0.6	0.6	0.6	0.9	0.9	0.8
Fraction within $\pm 50\%$	70.4	70.0	72.2	78.7	52.8	78.7	80.0	88.0	72.0

**Table 6.** Relative change 2000 *minus* 1980 (expressed in %, relative to 1980) for NO<sub>y</sub> wet deposition (wetnoy), NO<sub>x</sub> emissions (eminox) and total precipitation averaged over the region of interest. CICERO-OsloCTM2 uses the same climate for all simulations and therefore does not simulate any precipitation change.

Model	United States			Europe		
	wetnoy	eminox	precip	wetnoy	eminox	precip
CESM-CAM-superfast	4.8	0.6	4.2	-1.4	-14.2	0.5
CICERO-OsloCTM2	6.2	0.3	0	-7.3	-13.65	0
CMAM	7.3	3.8	-1.7	-12.7	-9.2	1.9
GEOSCCM	2.4	1.2	-0.6	-15.5	-13.6	0.3
GISS-E2-R	-0.8	-2.4	-0.3	-14.2	-11.3	2.9
GISS-E2-TOMAS	6.2	1.6	-0.3	-9.6	-10.8	2.9
MOCAGE	4.8	1.6	1.8	-3.1	-11.1	-3.3
NCAR-CAM3.5	6.5	1.6	2.4	-12.1	-13.2	0.8
STOC-HadAM3	9.9	1.8	2.6	-4.7	-10.6	4.1
UM-CAM	2.7	-2.0	-0.2	-4.9	-13.2	4.1
Multi-model mean	4.9	0.8	0.9	-8.9	-12.1	1.6

**Table 7.** Average MMM nitrogen ( $\text{NH}_x + \text{NO}_y$ ) deposition ( $\text{mg(N) m}^{-2} \text{yr}^{-1}$ ) over specific regions as defined in Lamarque et al. (2011).

Region	2000	RCP26 2100	RCP45 2100	RCP85 2100
Canada	203	150	148	201
USA	613	416	412	550
Mexico	412	464*	351	503*
C. America	264	313*	242	287*
Brazil	341	397*	299	465*
Rest of S. America	253	369*	253	359*
N. Africa	174	139	132	211*
W. Africa	396	524*	450*	573*
E. Africa	287	461*	355*	570*
S. Africa	297	389*	258	458*
W. Europe	768	448	467	662
C. Europe	1061	685	577	1256*
Turkey	693	541	512	657
Ukraine	859	584	415	1049*
Kazakhstan area	297	361*	201	328*
Russia	289	205	188	304*
Middle East	263	278*	190	383*
South Asia	728	1550*	1023*	1318*
Korea region	1058	921	751	894
East Asia	756	1021*	690	888*
Southeast Asia	661	827*	569	752*
Indonesia	658	694*	297	417
Japan	789	447	447	660
Oceania	126	133*	118	153*
Greenland	50	39	46	58*

\* indicates regions where the deposition increase with respect to 2000.

**Table 8.** Average MMM sulfur deposition ( $\text{mg(S)}\text{m}^{-2}\text{yr}^{-1}$ ) over specific regions as defined in Lamarque et al. (2011). The deposition does not increase in any of these regions with respect to 2000.

Region	2000	RCP26 2100	RCP45 2100	RCP85 2100
Canada	154	38	34	45
USA	506	65	71	75
Mexico	433	76	121	93
C. America	291	119	165	119
Brazil	120	52	67	69
Rest of S. America	163	90	116	112
N. Africa	145	48	96	67
W. Africa	133	103	115	126
E. Africa	123	73	89	97
S. Africa	157	148	79	133
W. Europe	534	98	141	107
C. Europe	1080	127	188	146
Turkey	727	136	205	130
Ukraine	794	80	129	98
Kazakhstan area	258	39	61	99
Russia	195	40	46	60
Middle East	313	54	73	155
South Asia	409	74	155	289
Korea region	1250	209	242	277
East Asia	670	71	93	108
Southeast Asia	416	132	162	182
Indonesia	390	292	270	249
Japan	922	414	515	431
Oceania	115	56	81	64
Greenland	42	21	18	25

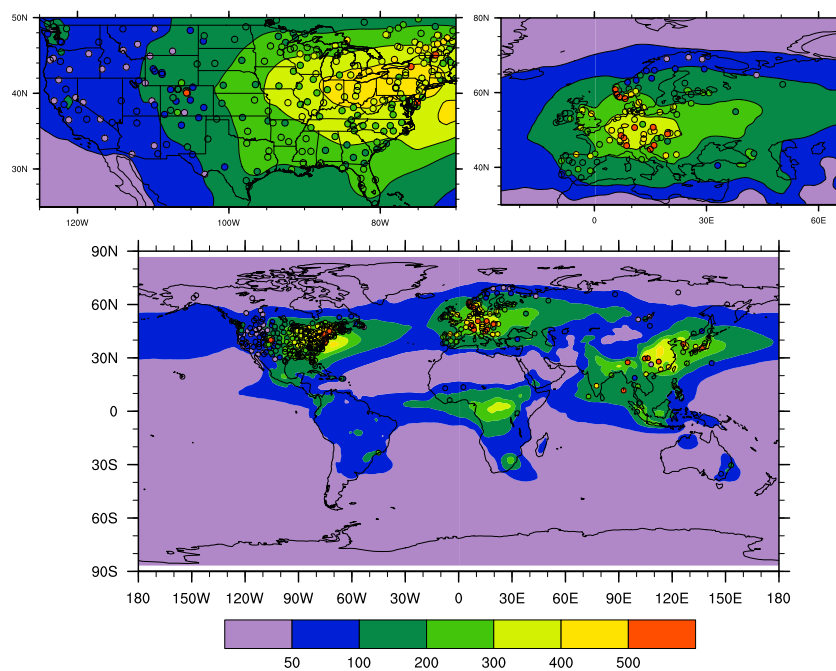


**Fig. 1a.** Nitrate wet deposition ( $\text{mg(N) m}^{-2} \text{yr}^{-1}$ ) for 2000. Contours are for the multi-model mean, filled circles are for the wet deposition network observations.

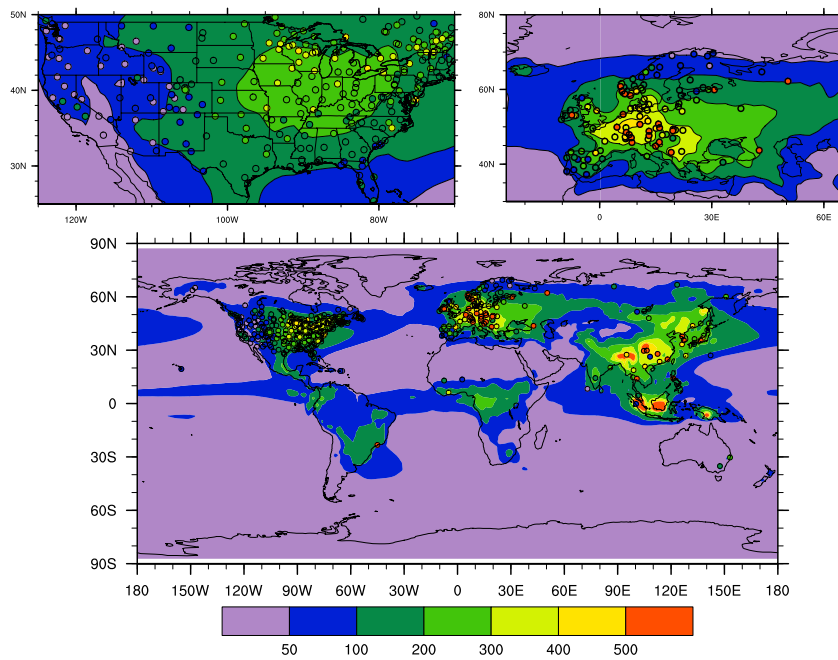


**Fig. 1b.** Ammonium wet deposition ( $\text{mg(N) m}^{-2} \text{ yr}^{-1}$ ) for 2000. Contours are for the multi-model mean, filled circles are for the wet deposition network observations.

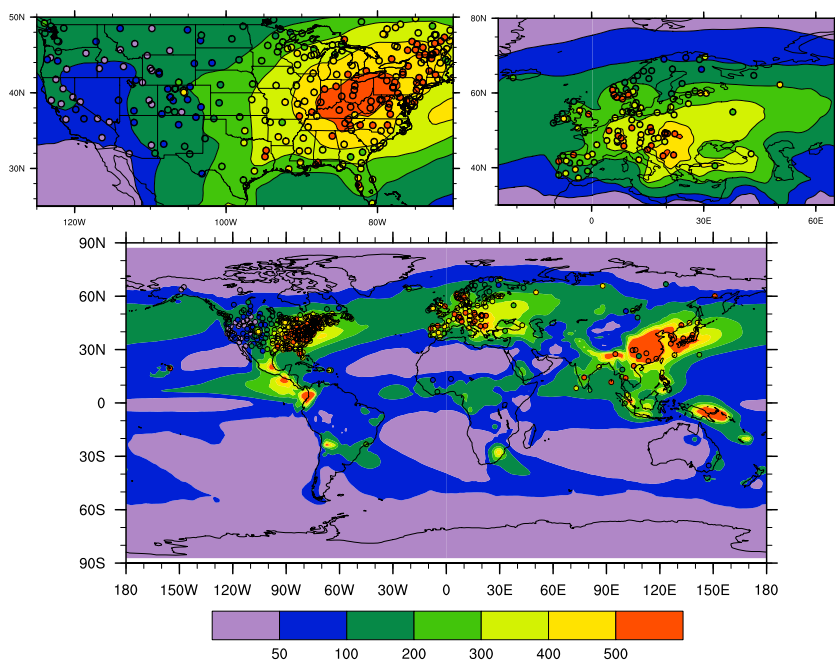


**Fig. 1c.** Sulfate wet deposition ( $\text{mg(S) m}^{-2} \text{ yr}^{-1}$ ) for 2000. Contours are for the multi-model mean, filled circles are for the wet deposition network observations.

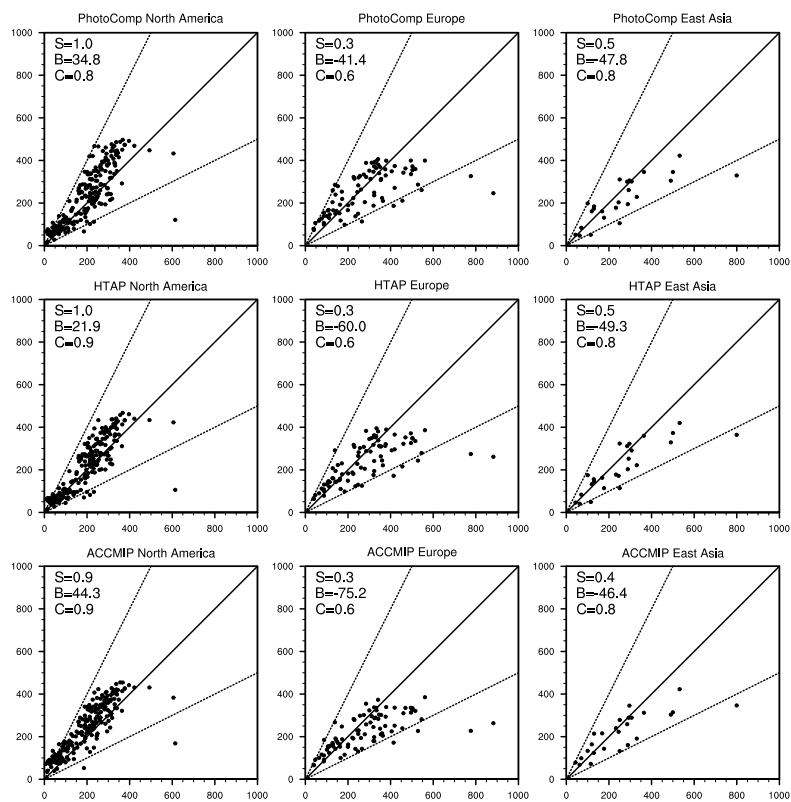


**Fig. 2a.** Scatterplot (X axis: observations, Y axis: multi-model mean) of nitrate wet deposition ( $\text{mg(N)}\text{m}^{-2}\text{yr}^{-1}$ ) over North America (left column), Europe (middle column) and East Asia (right column). Top row shows the model results from PhotoComp, middle row from HTAP and bottom row from this study. See text for details. S=slope, B=mean bias ( $\text{mg(N)}\text{m}^{-2}\text{yr}^{-1}$ ), C=correlation (see Table 5).

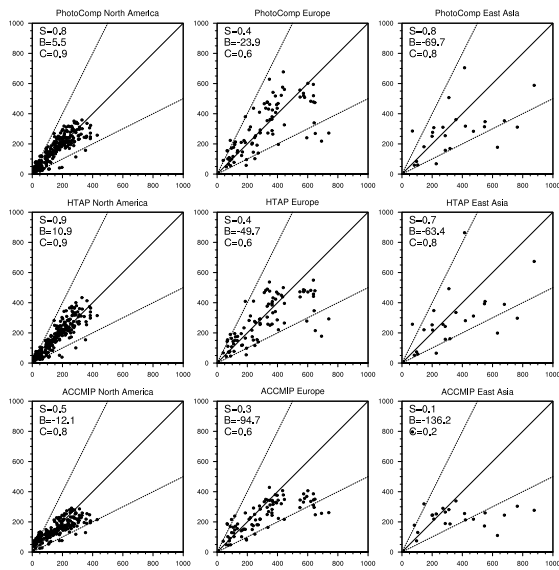


**Fig. 2b.** Scatterplot (X axis: observations, Y axis: multi-model mean) of ammonium wet deposition ( $\text{mg(N) m}^{-2} \text{yr}^{-1}$ ) over North America (left column), Europe (middle column) and East Asia (right column). Top row shows the model results from PhotoComp, middle row from HTAP and bottom row from this study. See text for details. S=slope, B=mean bias ( $\text{mg(N) m}^{-2} \text{yr}^{-1}$ ), C=correlation (see Table 5).

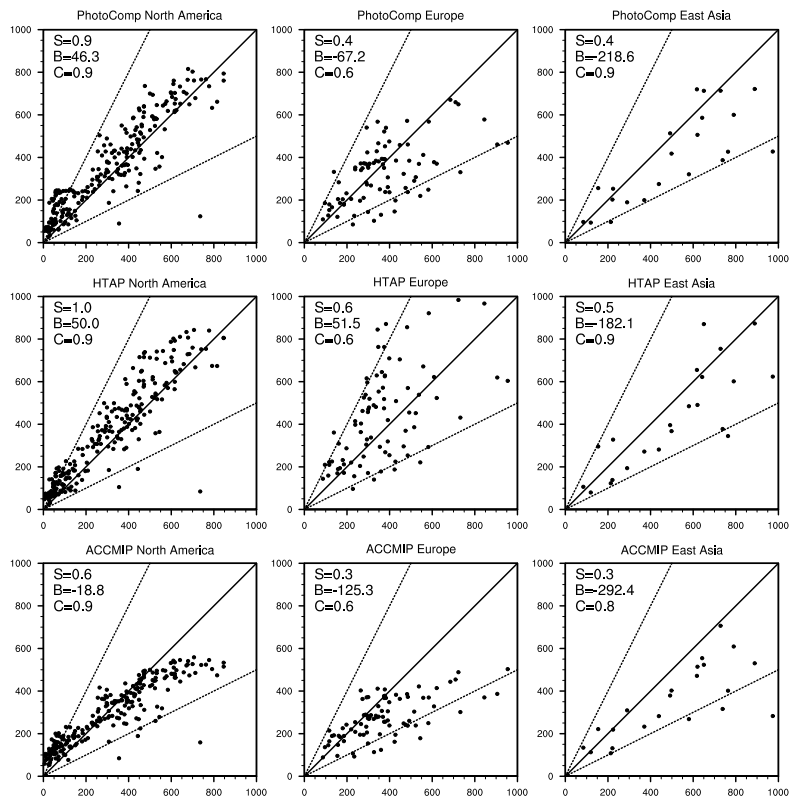


**Fig. 2c.** Scatterplot (X axis: observations, Y axis: multi-model mean) of sulfate wet deposition ( $\text{mg(S)}\text{m}^{-2}\text{yr}^{-1}$ ) over North America (left column), Europe (middle column) and East Asia (right column). Top row shows the model results from PhotoComp, middle row from HTAP and bottom row from this study. See text for details. S=slope, B=mean bias ( $\text{mg(S)}\text{m}^{-2}\text{yr}^{-1}$ ), C=correlation (see Table 5).

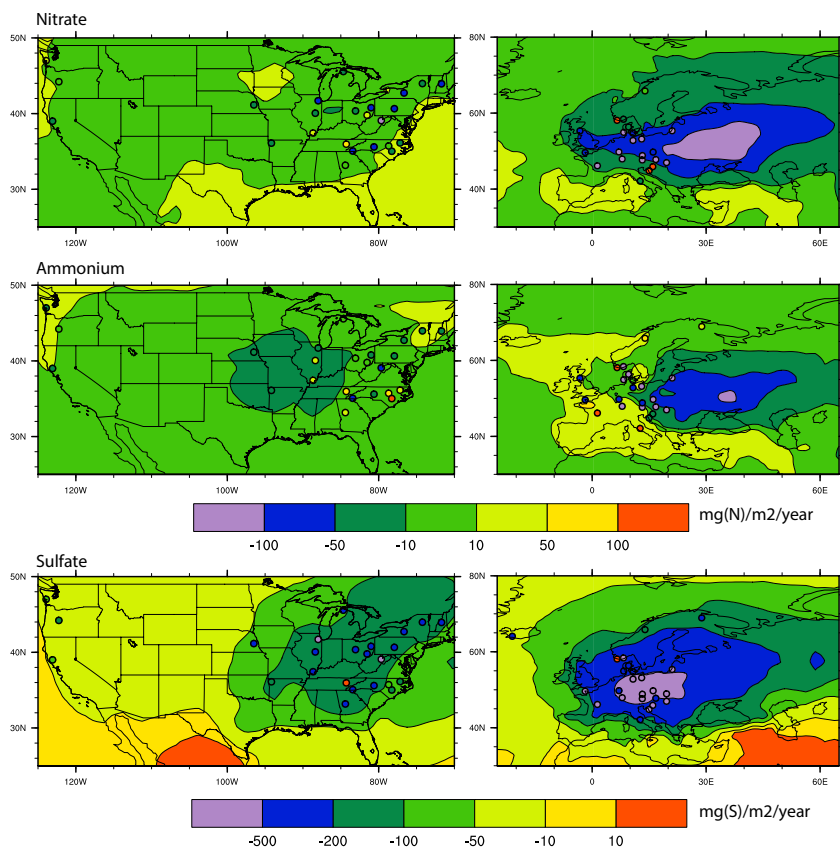


**Fig. 3.** Change in deposition (2000–1980) over the NADP (left column) and EMEP (right column) networks. Top row is for nitrate ( $\text{mg(N)}\text{m}^{-2}\text{yr}^{-1}$ ), middle row is for ammonium ( $\text{mg(N)}\text{m}^{-2}\text{yr}^{-1}$ ), bottom row is for sulfate ( $\text{mg(S)}\text{m}^{-2}\text{yr}^{-1}$ ). Contours are the MMM results, filled circles are the observations.

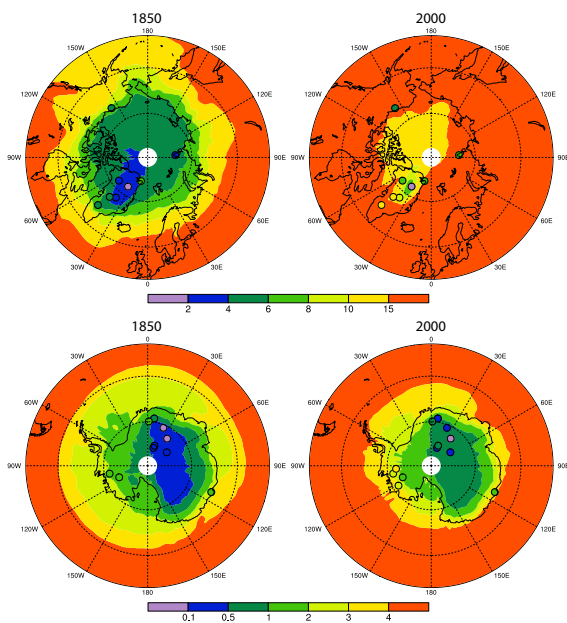


**Fig. 4a.** Nitrate deposition from ice-cores ( $\text{mg(N) m}^{-2} \text{yr}^{-1}$ , filled circles, see Table S5) and MMM for 1850 (left column) and 2000 (right column). Top panel is for the Arctic region, bottom panel is for the Antarctic region. Contours are the MMM results, filled circles are the observations. Note different color scales between top and bottom panels.

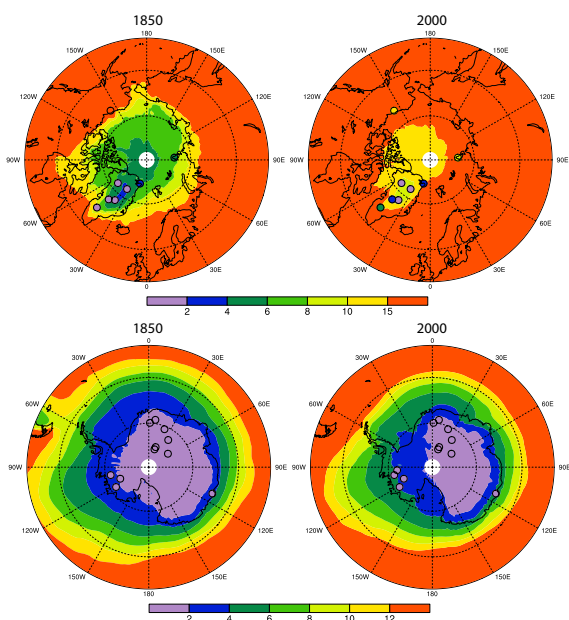


**Fig. 4b.** Ammonium deposition from ice-cores ( $\text{mg(N)} \text{m}^{-2} \text{yr}^{-1}$ , filled circles, see Table S5) and MMM for 1850 (left column) and 2000 (right column). Top panel is for the Arctic region, bottom panel is for the Antarctic region. Contours are the MMM results, filled circles are the observations. Note different color scales between top and bottom panels.

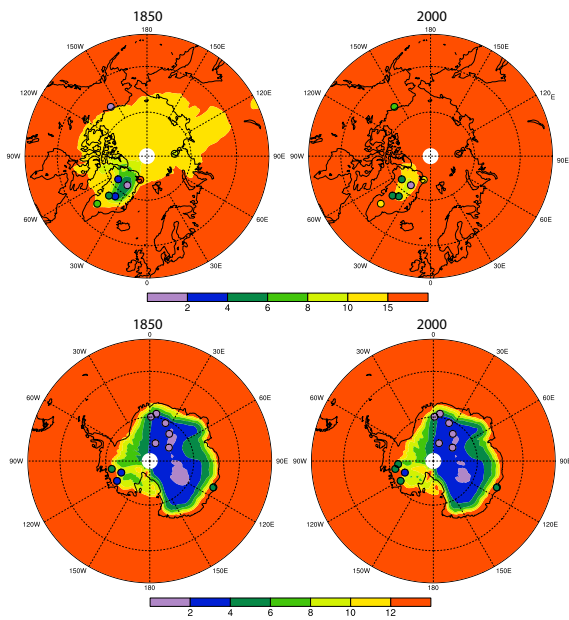


**Fig. 4c.** Sulfate deposition from ice-cores ( $\text{mg(S)} \text{m}^{-2} \text{yr}^{-1}$ , filled circles, see Table S5) and MMM for 1850 (left column) and 2000 (right column). Top panel is for the Arctic region, bottom panel is for the Antarctic region. Contours are the MMM results, filled circles are the observations. Note different color scales between top and bottom panels.

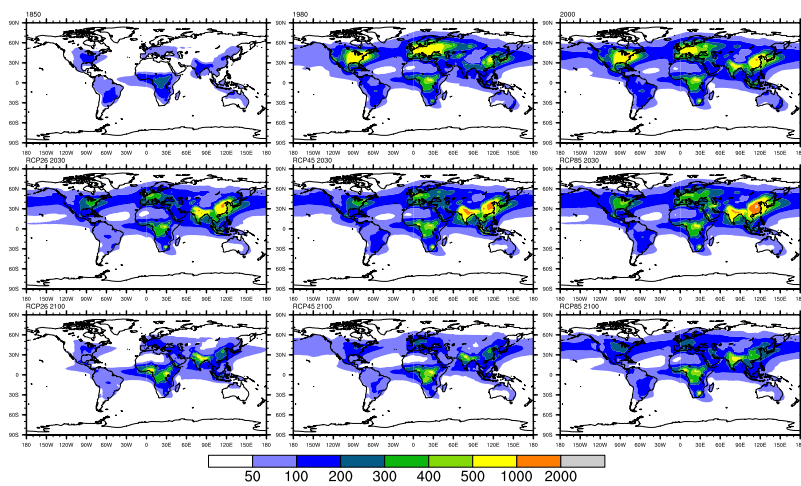


**Fig. 5a.** Total (wet + dry) NO<sub>y</sub> deposition 1850–2100 (mg(N) m<sup>-2</sup> yr<sup>-1</sup>). Top row shows 1850, 1980 and 2000. Middle row shows 2030 for RCP2.6, RCP4.5 and RCP8.5. Bottom row shows 2100 for RCP2.6, RCP4.5 and RCP8.5.

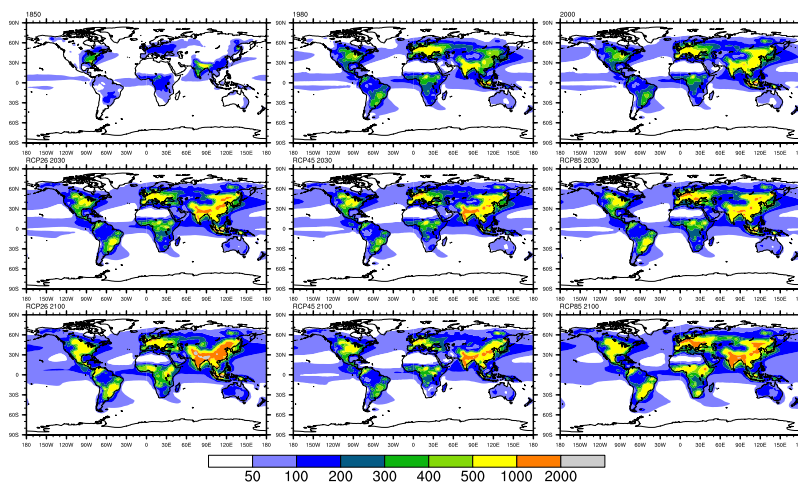


**Fig. 5b.** Total (wet + dry)  $\text{NH}_x$  deposition 1850–2100 ( $\text{mg(N) m}^{-2} \text{yr}^{-1}$ ). Top row shows 1850, 1980 and 2000. Middle row shows 2030 for RCP2.6, RCP4.5 and RCP8.5. Bottom row shows 2100 for RCP2.6, RCP4.5 and RCP8.5.

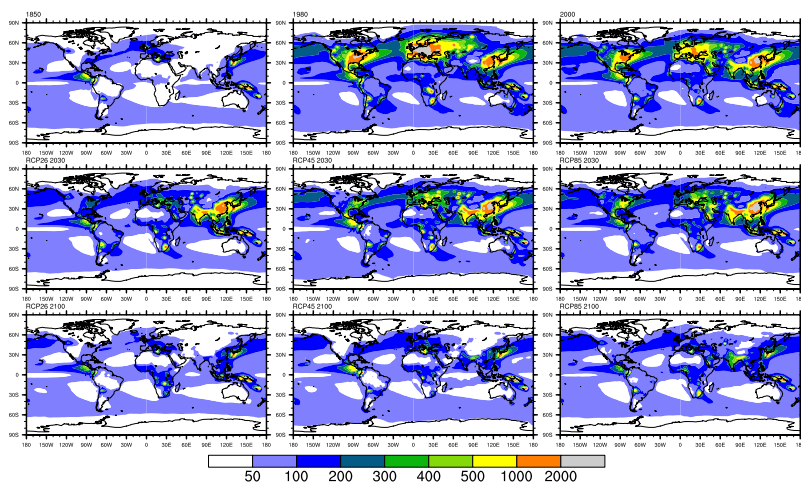


**Fig. 5c.** Total (wet + dry)  $\text{SO}_x$  deposition 1850–2100 ( $\text{mg(S)}\text{m}^{-2}\text{yr}^{-1}$ ). Top row shows 1850, 1980 and 2000. Middle row shows 2030 for RCP2.6, RCP4.5 and RCP8.5. Bottom row shows 2100 for RCP2.6, RCP4.5 and RCP8.5.

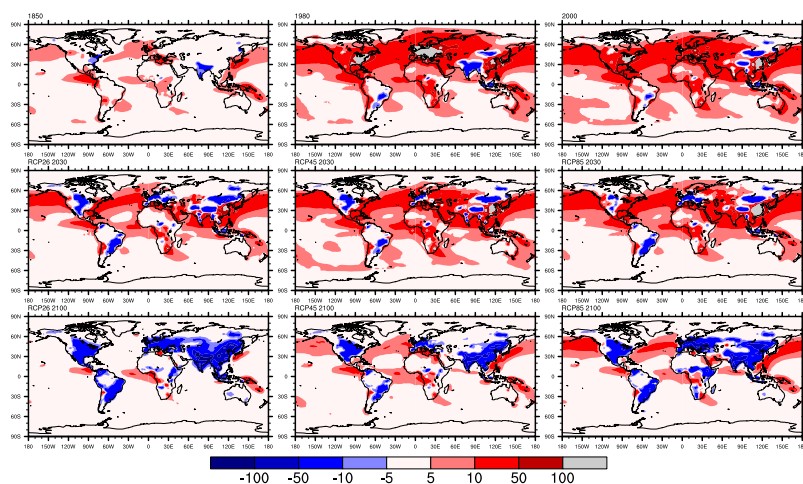


**Fig. 6.** Time evolution of added deposition acidity ( $10^{-6} \text{ mol m}^{-2} \text{ yr}^{-1}$ ) computed as  $2 \cdot \text{SO}_x + \text{NO}_y - \text{NH}_x$ . Blue regions indicate areas where deposition is more basic than it would have been without those respective emissions. Top row shows 1850, 1980 and 2000. Middle row shows 2030 for RCP2.6, RCP4.5 and RCP8.5. Bottom row shows 2100 for RCP2.6, RCP4.5 and RCP8.5.

Supplement to: Multi-model mean nitrogen and sulfur deposition from the Atmospheric Chemistry and Climate Model Intercomparison Project (ACCMIP): evaluation and historical and projected changes by Lamarque et al.

This supplement contains

Table S1: Model description, adapted from Lamarque et al. (2013)

Table S2: Regional mean and standard deviation (amongst models) of dry deposition, wet deposition and associated  $\text{NO}_x$  emissions over the 1850-2000 (Table S2a), 2030 (Table S2b) and 2100 (Table S2c)

Table S3: Regional mean and standard deviation (amongst models) of dry deposition, wet deposition and associated  $\text{NH}_x$  emissions over the 1850-2000 (Table S3a), 2030 (Table S3b) and 2100 (Table S3c)

Table S4: Regional mean and standard deviation (amongst models) of dry deposition, wet deposition and associated  $\text{SO}_x$  emissions over the 1850-2000 (Table S4a), 2030 (Table S4b) and 2100 (Table S4c)

Table S5: Contribution of each model to deposition diagnostics for each time-slice

Table S6: Geographical information on ice-core locations used in this study

Figure S1a. Change (2000-1980) in anthropogenic emissions of NO over the United States and Europe.

Figure S1b. Change (2000-1980) in anthropogenic emissions of  $\text{NH}_3$  over the United States and Europe.

Figure S1c. Change (2000-1980) in anthropogenic emissions of  $\text{SO}_2$  over the United States and Europe.

Only the anthropogenic portion of the emissions is shown in Fig.1 since that is the largest contributor to changes over the 1980-2000 period.

Figure S2. Comparison of the precipitation change in the ACCMIP MMM and in the CMAP precipitation dataset (Xie and Arkin, 1997).

Figure S3. Comparison of annual total precipitation in the ACCMIP MMM against the gauge-based precipitation measurements that are available for the period of 1995 to 2004 and cover large areas in the Arctic (Yang et al., 2005), available [http://ine.uaf.edu/werc/people/yang/yang\\_files/MonthlySum/](http://ine.uaf.edu/werc/people/yang/yang_files/MonthlySum/)

Figure S4. Inter-model standard deviation (in %) of the  $\text{NO}_y$  wet deposition. The standard deviation is only shown for regions where deposition is larger than  $50 \text{ mg(N)}/\text{m}^2/\text{year}$  (see Fig. 5a). The number of models used for each time slice is shown in Table S2.

Figure S5. Multi-model mean evolution of a) total nitrogen and b) sulfur deposition (in  $\text{mg(N or S)}/\text{m}^2/\text{yr}$ ) relative to year 2000.

## References

- Josse, B., Simon, P., Peuch, V. H.: Radon global simulations with the multiscale chemistry and transport model MOCAGE, *Tellus-B*, 56, 339-356, 2004.
- Koch, D., G.A. Schmidt, and C.V. Field. Sulfur, sea salt and radionuclide aerosols in GISS ModelE. *J. Geophys. Res.*, **111**, D06206, doi:10.1029/2004JD005550, 2006.
- Lamarque, J.-F., G. P. Kyle, M. Meinshausen, K. Riahi, S. J. Smith, D. P. van Vuuren, A. Conley, F. Vitt. Global and regional evolution of short-lived radiatively-active gases and aerosols in the Representative Concentration Pathways. *Climatic Change*, doi:10.1007/s10584-011-0155-0, 2011.
- Lamarque, J.-F., Shindell, D. T., Josse, B., Young, P. J., Cionni, I., Eyring, V., Bergmann, D., Cameron-Smith, P., Collins, W. J., Doherty, R., Dalsoren, S., Faluvegi, G., Folberth, G., Ghan, S. J., Horowitz, L. W., Lee, Y. H., MacKenzie, I. A., Nagashima, T., Naik, V., Plummer, D., Righi, M., Rumbold, S., Schulz, M., Skeie, R. B., Stevenson, D. S., Strode, S., Sudo, K., Szopa, S., Voulgarakis, A., and Zeng, G.: The Atmospheric Chemistry and Climate Model Intercomparison Project (ACCMIP): overview and description of models, simulations and climate diagnostics, *Geosci. Model Dev.*, 6, 179-206, doi:10.5194/gmd-6-179-2013, 2013.
- Lamarque, J.-F., L. K. Emmons, P. G. Hess, D. E. Kinnison, S. Tilmes, F. Vitt, C. L. Heald, E. A. Holland, P. H. Lauritzen, J. Neu, J. J. Orlando, P. Rasch, G. Tyndall. CAM-chem: description and evaluation of interactive atmospheric chemistry in CESM. *Geosci. Mod. Dev.*, 5, 369-411, doi:10.5194/gmd-5-369-2012, 2012.
- Lee, Y. H., and Adams, P. J.: A Fast and Efficient Version of the Two-Moment Aerosol Sectional (TOMAS) Global Aerosol Microphysics Model, *Aerosol Science and Technology*, 46, 678-689, 10.1080/02786826.2011.643259, 2011.
- Liu, X., R. C. Easter, S. J. Ghan, R. Zaveri, P. Rasch, X. Shi, J.-F. Lamarque, A. Gettelman, H. Morrison, F. Vitt, A. Conley, S. Park, R. Neale, C. Hannay, A. M. L. Ekman, P. Hess, N. Mahowald, W. Collins, M. J. Iacono, C. S. Bretherton, M. G. Flanner, and D. Mitchell, 2012: Toward a minimal representation of aerosols in climate models: Description and evaluation in the Community Atmosphere Model CAM5. *Geosci. Model Dev.*, 5, 709-739, doi:10.5194/gmd-5-709-2012.
- Oman, L.D., J. R. Ziemke, A. R. Douglass, D.W. Waugh, C. Lang, J.M. Rodriguez, and J.E. Nielsen, The response of tropical tropospheric ozone to ENSO, *Geophys. Res. Lett.*, 38, L13706, doi:10.1029/2011GL047865, 2011.
- Scinocca, J. F., N. A. McFarlane, M. Lazare, J. Li and D. Plummer, Technical Note: The CCCma third generation AGCM and its extension into the middle atmosphere, *Atmos. Chem. Phys.*, 8, 7055-7074, doi:10.5194/acp-8-7055-2008, 2008.

Shindell, D. T., Pechony, O., Voulgarakis, A., Faluvegi, G., Nazarenko, L., Lamarque, J.-F., Bowman, K., Milly, G., Kovari, B., Ruedy, R., and Schmidt, G.: Interactive ozone and methane chemistry in GISS-E2 historical and future climate simulations, *Atmos. Chem. Phys.*, 13, 2653-2689, doi:10.5194/acp-13-2653-2013, 2013.

Skeie, R. B., Berntsen, T. K., Myhre, G., Tanaka, K., Kvalevag, M. M. et al.: Anthropogenic radiative forcing time series from pre-industrial times until 2010, *Atmospheric Chemistry and Physics*, 11(22), 11827-11857, 2011.

Stevenson, D. S., R. M. Doherty, M. G. Sanderson, W. J. Collins, C. E. Johnson, and R. G. Derwent, Radiative forcing from aircraft NO<sub>x</sub> emissions: Mechanisms and seasonal dependence, *J. Geophys. Res.*, 109, D17307, doi:10.1029/2004JD004759, 2004.

Teyssède, H., Michou, M., Clark, H. L., Josse, B., Karcher, F., Olivie, D., Peuch, V.-H., Saint-Martin, D., Cariolle, D., Attié, J.-L., Nédélec, P., Ricaud, P., Thouret, V., van der A, R. J., Volz-Thomas, A., and Chéroux, F.: A new tropospheric and stratospheric Chemistry and Transport Model MOCAGE-Climat for multi-year studies: evaluation of the present-day climatology and sensitivity to surface processes, *Atmos. Chem. Phys.*, 7, 5815-5860, doi:10.5194/acp-7-5815-2007, 2007.

Xie, P., and P.A. Arkin, 1997: Global precipitation: A 17-year monthly analysis based on gauge observations, satellite estimates, and numerical model outputs. *Bull. Amer. Meteor. Soc.*, 78, 2539 - 2558.

Yang, D., D. Kane, Z. Zhang, D. Legates and B. Goodison. Bias-corrections of long-term (1973-2004) daily precipitation data over the northern regions, *Geophysical Research Letters*, vol. 32, L19501, doi:10.1029/2005GL024057, 2005.

Zeng, G., Pyle, J. A., and Young, P. J.: Impact of climate change on tropospheric ozone and its global budgets, *Atmos. Chem. Phys.*, 8, 369–387, doi:http://dx.doi.org/10.5194/acp-8-369-200810.5194/acp-8-369-2008, 2008.

Zeng, G., Morgenstern, O., Braesicke, P., and Pyle, J. A.: Impact of stratospheric ozone recovery on tropospheric ozone and its budget, *Geophys. Res. Lett.*, 37, L09805, doi:http://dx.doi.org/10.1029/2010GL04281210.1029/2010GL042812, 2010.

Model	Modelling Center	Model Contact	Resolution (lat/lon/lev), Top Level	NOy deposition	NHx deposition	SOx deposition	Reference
<b>CESM-CAM-Superfast</b>	LLNL, USA	Dan Bergmann, Philip Cameron-Smith	1.875/2.5/L26, 3.5hPa	X		X	Lamarque et al, 2012
<b>CICERO-OsloCTM2</b>	CICERO, Norway	Stig Dalsoren, Ragnhild Skeie	2.8/2.6/L60, 0.11 hPa	X	X	X	Skeie et al., 2011
<b>CMAM</b>	CCCMA, Environment Canada, Canada	David Plummer	3.75/3.75/L71, 0.00081hPa	X			Scinocca et al, 2008
<b>GEOSCCM</b>	NASA GSFC, USA	Sarah Strode	2/2.5/L72, 0.01hPa	X			Oman et al, 2011
<b>GISS-E2-R</b>	NASA-GISS, USA	Drew Shindell, Greg Faluvegi,	2/2.5/L40, 0.14hPa	X	X	X	Koch et al, 2006 ; Shindell et al, 2013
<b>GISS-E2-R-TOMAS</b>	NASA-GISS, USA	Drew Shindell, Greg Faluvegi, Yunha Lee	2/2.5/L40, 0.14hPa	X			Shindell et al, 2013; Lee and Adams, 2011
<b>MOCAGE</b>	GAME/CNRM, MétéoFrance, France	Béatrice Josse	2.0/2.0/L47, 6.9 hpa	X			Josse et al, 2004 Teyssède et al, 2007
<b>NCAR-CAM3.5</b>	NCAR ESL, USA	Jean-François Lamarque	1.875/2.5/L26, 3.5hPa	X	X	X	Lamarque et al, 2011 Lamarque et al, 2012
<b>NCAR-CAM5.1</b>	PNNL, USA	Steven Ghan	1.875/2.5/L30, 3.5hPa			X	Liu et al, 2012
<b>STOC-HadAM3</b>	University of Edinburgh, United Kingdom	Ian McKenzie, David Stevenson, Ruth Doherty	5.0/5.0/L19 50hPa	X	X	X	Stevenson et al, 2004
<b>UM-CAM</b>	NIWA, New Zealand	Guang Zeng	2.5/3.75/L19, 4.6hPa	X			Zeng et al, 2008, 2010

**Table S1.** Model description summary, adapted from Lamarque et al. (2013).

	historical					
	1850		1980		2000	
	mean	sdev	mean	sdev	mean	sdev
dry deposition						
North America	0.5	0.2	2.8	0.8	2.9	0.8
Central + South America	0.5	0.3	0.9	0.4	1.0	0.4
Africa	1.3	0.6	2.6	0.7	2.7	0.7
Europe	0.2	0.1	1.6	0.5	1.4	0.4
Former USSR + Middle East	0.4	0.1	2.8	0.8	2.4	0.6
Asia	0.6	0.3	2.1	0.6	3.6	1.1
Oceania	0.2	0.1	0.3	0.1	0.3	0.1
Continents	3.8	1.6	13.1	3.5	14.4	3.8
Ocean	1.4	0.6	5.3	2.0	6.4	2.3
Global	5.2	1.8	18.4	5.1	20.7	5.6
wet deposition						
North America	0.6	0.2	2.7	0.5	2.9	0.6
Central + South America	0.9	0.4	1.3	0.5	1.5	0.6
Africa	1.6	0.4	2.7	0.5	2.8	0.5
Europe	0.2	0.0	1.4	0.4	1.3	0.3
Former USSR + Middle East	0.5	0.1	2.9	0.7	2.5	0.6
Asia	1.1	0.3	2.6	0.5	4.0	0.8
Oceania	0.3	0.1	0.4	0.1	0.4	0.1
Continents	5.3	1.4	14.0	2.9	15.4	3.0
Ocean	5.8	2.4	12.3	3.2	14.5	3.9
Global	11.1	2.8	26.3	4.3	30.0	4.7
emissions						
North America	1.6	0.3	7.7	0.4	7.9	0.4
Central + South America	2.4	1.0	3.5	1.0	3.9	0.9
Africa	4.0	1.2	6.4	1.0	6.5	1.0
Europe	0.4	0.1	4.7	0.2	4.1	0.2
Former USSR + Middle East	1.0	0.3	5.8	0.3	4.8	0.3
Asia	2.3	0.9	5.9	0.9	9.8	1.0
Oceania	0.8	0.2	1.1	0.2	1.2	0.2
Continents	12.5	3.9	35.0	3.4	38.2	3.5
Ocean	1.4	0.8	6.0	1.3	8.1	1.7
Global	13.9	4.5	41.0	3.9	46.3	4.2
Number of models	10		10		10	

Table S2a. Multi-model mean and standard deviation regional deposition and emission (Tg(N)/yr) from NO<sub>x</sub> emissions for the historical period.

	2030					
	RCP26		RCP45		RCP85	
dry deposition	mean	sdev	mean	sdev	mean	sdev
North America	1.3	0.4	1.4	0.4	1.8	0.5
Central + South America	0.6	0.3	0.9	0.5	1.0	0.5
Africa	2.4	0.6	3.2	0.9	3.1	0.8
Europe	0.9	0.3	0.9	0.3	1.0	0.3
Former USSR + Middle East	1.7	0.4	2.2	0.7	2.8	0.8
Asia	4.2	1.5	5.4	1.9	6.4	1.9
Oceania	0.2	0.1	0.3	0.1	0.3	0.1
Continents	11.3	3.4	14.3	4.5	16.3	4.6
Ocean	5.7	1.9	6.0	2.1	6.8	2.0
Global	17.0	5.1	20.3	6.3	23.1	6.3

	mean	sdev	mean	sdev	mean	sdev
wet deposition						
North America	1.4	0.2	1.4	0.3	1.8	0.2
Central + South America	1.0	0.3	1.1	0.4	1.2	0.3
Africa	2.5	0.2	2.7	0.1	2.8	0.3
Europe	0.7	0.2	0.8	0.2	0.8	0.2
Former USSR + Middle East	1.6	0.3	1.9	0.4	2.3	0.4
Asia	4.2	0.8	4.9	0.6	5.6	0.8
Oceania	0.3	0.1	0.3	0.1	0.3	0.1
Continents	11.8	1.3	13.1	1.3	14.9	1.5
Ocean	13.7	4.1	14.5	5.4	15.0	4.4
Global	25.4	5.0	27.6	6.6	29.9	5.4

	mean	sdev	mean	sdev	mean	sdev
emissions						
North America	3.6	0.5	3.4	0.5	4.3	0.5
Central + South America	3.0	1.1	3.3	1.0	3.6	1.1
Africa	6.5	1.4	6.8	1.2	7.1	1.3
Europe	2.3	0.2	2.1	0.2	2.4	0.3
Former USSR + Middle East	3.3	0.3	4.0	0.3	5.4	0.4
Asia	11.4	1.6	12.2	1.8	15.3	1.3
Oceania	0.8	0.2	0.8	0.3	0.9	0.2
Continents	30.9	5.0	32.6	5.1	39.0	4.9
Ocean	8.2	1.3	8.6	0.6	9.1	1.3
Global	39.1	5.9	41.1	5.3	48.1	5.8
Number of models	6		4		7	

Table S2b. Multi-model mean and standard deviation regional deposition and emission (Tg(N)/yr) from NO<sub>x</sub> emissions for 2030.

	2100					
	RCP26		RCP45		RCP85	
dry deposition	mean	sdev	mean	sdev	mean	sdev
North America	0.5	0.2	0.8	0.3	1.1	0.4
Central + South America	0.6	0.3	0.7	0.4	0.8	0.4
Africa	2.4	0.7	2.7	1.0	2.9	1.0
Europe	0.3	0.1	0.5	0.2	0.6	0.2
Former USSR + Middle East	1.0	0.3	1.0	0.4	1.6	0.5
Asia	2.0	0.8	1.9	0.8	2.5	0.8
Oceania	0.1	0.1	0.2	0.1	0.2	0.1
Continents	6.8	2.2	7.8	2.9	9.7	3.2
Ocean	2.6	1.0	3.3	1.1	4.7	1.5
Global	9.4	3.2	11.1	3.8	14.4	4.4

	mean	sdev	mean	sdev	mean	sdev
wet deposition						
North America	0.7	0.2	1.0	0.2	1.4	0.2
Central + South America	0.9	0.3	0.9	0.3	1.1	0.3
Africa	2.7	0.3	2.5	0.1	3.0	0.4
Europe	0.3	0.1	0.5	0.1	0.5	0.1
Former USSR + Middle East	0.9	0.2	1.1	0.2	1.6	0.3
Asia	2.2	0.5	2.2	0.4	3.0	0.5
Oceania	0.2	0.1	0.3	0.1	0.3	0.1
Continents	7.9	1.0	8.4	1.0	11.0	1.3
Ocean	8.8	3.4	10.2	4.5	12.4	4.1
Global	16.7	4.2	18.6	5.5	23.4	4.9

	mean	sdev	mean	sdev	mean	sdev
emissions						
North America	1.5	0.4	2.2	0.5	3.0	0.7
Central + South America	2.8	1.1	2.4	1.1	3.0	1.3
Africa	7.3	1.4	6.1	1.4	7.2	1.7
Europe	0.8	0.2	1.2	0.2	1.4	0.3
Former USSR + Middle East	2.1	0.3	1.9	0.4	3.3	0.5
Asia	5.9	1.4	5.0	1.6	6.9	1.6
Oceania	0.6	0.2	0.7	0.3	0.8	0.3
Continents	21.1	4.9	19.5	5.4	25.6	6.1
Ocean	2.9	1.1	5.3	0.6	7.8	1.3
Global	24.0	5.8	24.8	5.8	33.4	7.1
Number of models	6		4		7	

Table S2c. Multi-model mean and standard deviation regional deposition and emission (Tg(N)/yr) from NO<sub>x</sub> emissions for 2100.

	historical					
	1850		1980		2000	
	mean	sdev	mean	sdev	mean	sdev
dry deposition						
North America	0.9	0.3	1.4	0.5	1.6	0.5
Central + South America	0.6	0.2	1.9	0.3	1.8	0.3
Africa	1.1	0.3	2.5	0.4	2.2	0.4
Europe	0.2	0.1	1.0	0.3	1.4	0.4
Former USSR + Middle East	0.6	0.2	1.6	0.7	1.8	0.7
Asia	1.5	0.3	4.5	1.1	5.5	1.4
Oceania	0.2	0.1	0.3	0.1	0.3	0.1
Continents	5.2	1.2	13.3	3.1	14.6	3.4
Ocean	3.0	1.2	4.5	1.9	4.9	2.0
Global	8.2	2.2	17.8	4.6	19.5	5.0

	mean	sdev	mean	sdev	mean	sdev
wet deposition						
North America	0.9	0.2	2.1	0.5	2.2	0.4
Central + South America	0.7	0.3	1.8	0.6	1.7	0.6
Africa	0.9	0.4	2.1	0.7	1.9	0.6
Europe	0.3	0.0	1.3	0.3	1.4	0.2
Former USSR + Middle East	0.7	0.2	2.6	0.8	2.8	0.7
Asia	1.3	0.5	4.5	1.8	6.0	2.1
Oceania	0.2	0.1	0.3	0.1	0.3	0.1
Continents	4.9	1.5	14.8	3.2	16.3	3.6
Ocean	7.2	1.5	11.9	2.4	13.2	2.6
Global	12.1	2.3	26.7	4.3	29.5	4.8

	mean	sdev	mean	sdev	mean	sdev
emissions						
North America	2.1	0.5	3.9	0.2	4.1	0.3
Central + South America	0.8	0.4	4.2	0.4	3.8	0.4
Africa	2.2	0.4	5.8	0.7	5.0	0.7
Europe	0.6	0.1	3.3	0.1	4.1	0.1
Former USSR + Middle East	1.3	0.3	4.0	0.2	4.2	0.6
Asia	3.3	0.2	12.1	0.9	15.5	1.0
Oceania	0.5	0.1	0.9	0.1	0.8	0.1
Continents	10.7	1.3	34.1	1.1	37.5	1.7
Ocean	6.8	3.1	8.5	3.4	9.0	3.5
Global	17.4	4.3	42.6	4.2	46.5	4.9
Number of models	5		5		5	

Table S3a. Multi-model mean and standard deviation regional deposition and emission (Tg(N)/yr) from NH<sub>x</sub> emissions for the historical period.

	2030					
	RCP26		RCP45		RCP85	
dry deposition	mean	sdev	mean	sdev	mean	sdev
North America	2.7	0.3	2.4	0.0	2.7	0.3
Central + South America	2.6	0.3	2.0	0.2	2.8	0.3
Africa	3.2	0.3	2.5	0.1	3.2	0.3
Europe	1.7	0.4	1.5	0.2	2.2	0.5
Former USSR + Middle East	2.7	0.7	2.0	0.1	3.1	0.8
Asia	8.8	1.9	6.5	0.5	7.7	1.8
Oceania	0.5	0.1	0.3	0.0	0.5	0.1
Continents	22.2	3.6	17.2	0.4	22.1	3.9
Ocean	7.8	3.2	6.0	2.7	7.6	2.9
Global	30.0	5.6	23.1	2.3	29.7	5.6

	mean	sdev	mean	sdev	mean	sdev
wet deposition						
North America	2.0	0.4	2.2	0.2	2.2	0.3
Central + South America	2.0	0.9	1.9	0.7	2.2	1.0
Africa	2.4	0.9	2.2	0.6	2.4	0.8
Europe	1.0	0.3	1.2	0.3	1.3	0.4
Former USSR + Middle East	2.2	0.5	2.7	0.1	2.8	0.7
Asia	7.3	3.5	7.0	2.5	6.9	2.6
Oceania	0.3	0.1	0.3	0.1	0.3	0.1
Continents	17.3	6.4	17.6	4.5	18.2	5.5
Ocean	12.8	1.4	12.8	0.9	13.2	1.5
Global	30.0	6.3	30.4	3.6	31.4	5.7

	mean	sdev	mean	sdev	mean	sdev
emissions						
North America	5.1	0.1	5.1	0.1	5.4	0.0
Central + South America	5.3	0.3	4.4	0.3	5.8	0.3
Africa	6.7	0.3	5.2	0.3	6.7	0.3
Europe	3.8	0.1	4.1	0.0	5.0	0.1
Former USSR + Middle East	5.1	0.2	4.7	0.1	6.2	0.2
Asia	22.1	0.6	19.5	0.1	19.9	0.5
Oceania	1.0	0.0	0.9	0.0	1.0	0.0
Continents	49.0	0.9	43.9	0.9	50.0	0.9
Ocean	11.4	2.0	9.7	0.6	11.8	2.0
Global	60.4	1.5	53.6	0.4	61.7	1.5
Number of models	3		2		3	

Table S3b. Multi-model mean and standard deviation regional deposition and emission (Tg(N)/yr) from NH<sub>x</sub> emissions for 2030.

	2100					
	RCP26		RCP45		RCP85	
dry deposition	mean	sdev	mean	sdev	mean	sdev
North America	3.6	0.5	2.8	0.2	4.0	0.4
Central + South America	3.7	0.6	2.1	0.4	3.6	0.6
Africa	4.6	0.6	2.8	0.3	5.1	0.7
Europe	1.8	0.3	1.3	0.1	2.7	0.5
Former USSR + Middle East	3.7	0.7	2.1	0.1	4.4	1.0
Asia	13.5	2.8	6.9	0.5	10.1	1.9
Oceania	0.6	0.1	0.4	0.0	0.7	0.1
Continents	31.4	4.5	18.4	0.3	30.7	4.5
Ocean	11.3	5.8	7.2	4.0	11.0	5.4
Global	42.7	8.4	25.6	4.3	41.6	7.7

	mean	sdev	mean	sdev	mean	sdev
wet deposition						
North America	2.3	0.9	2.2	0.6	2.7	0.9
Central + South America	2.7	1.6	2.0	0.9	2.7	1.6
Africa	3.1	1.5	2.2	1.0	3.9	2.3
Europe	1.0	0.5	1.0	0.4	1.4	0.8
Former USSR + Middle East	2.3	0.8	2.0	0.3	3.0	0.9
Asia	9.5	7.0	6.6	4.2	7.3	4.4
Oceania	0.4	0.2	0.4	0.1	0.4	0.2
Continents	21.3	12.0	16.4	7.5	21.5	11.0
Ocean	13.7	1.6	11.6	0.7	14.0	1.8
Global	34.9	12.0	28.0	6.9	35.6	11.0

	mean	sdev	mean	sdev	mean	sdev
emissions						
North America	6.2	0.1	5.3	0.1	7.2	0.1
Central + South America	7.2	0.4	4.4	0.3	7.3	0.3
Africa	9.1	0.2	5.8	0.3	11.4	0.3
Europe	3.3	0.0	3.2	0.0	5.4	0.1
Former USSR + Middle East	6.4	0.2	4.4	0.1	8.0	0.2
Asia	30.6	0.8	18.4	0.0	23.2	0.5
Oceania	1.3	0.0	1.0	0.0	1.4	0.0
Continents	64.0	1.1	42.4	0.8	63.8	1.1
Ocean	12.6	2.5	9.6	0.6	12.7	2.3
Global	76.6	1.7	52.0	0.3	76.5	1.7
Number of models	3		2		3	

Table S3c. Multi-model mean and standard deviation regional deposition and emission (Tg(N)/yr) from NH<sub>x</sub> emissions for 2100.

	historical					
	1850		1980		2000	
	mean	sdev	mean	sdev	mean	sdev
dry deposition						
North America	0.4	0.3	6.2	1.1	4.1	1.0
Central + South America	0.3	0.1	1.3	0.3	1.1	0.3
Africa	0.5	0.1	2.4	0.4	2.1	0.4
Europe	0.4	0.2	8.9	1.3	2.7	0.6
Former USSR + Middle East	0.3	0.2	5.2	0.5	3.7	0.7
Asia	0.5	0.2	4.7	1.0	6.8	1.6
Oceania	0.2	0.1	0.5	0.1	0.6	0.1
Continents	2.7	1.1	29.2	4.3	21.0	4.6
Ocean	8.4	3.9	17.7	6.6	15.7	5.8
Global	11.1	4.8	46.8	9.7	36.7	9.5

	mean	sdev	mean	sdev	mean	sdev
wet deposition						
North America	0.8	0.3	4.7	0.8	4.1	0.8
Central + South America	1.3	0.4	2.1	0.5	2.2	0.5
Africa	0.7	0.2	2.3	0.4	2.3	0.4
Europe	0.5	0.2	3.3	0.7	1.8	0.5
Former USSR + Middle East	0.8	0.2	6.0	1.6	4.4	1.0
Asia	1.7	0.3	5.1	0.9	8.0	1.8
Oceania	0.4	0.0	0.6	0.1	0.6	0.1
Continents	6.3	0.9	24.1	4.7	23.3	4.7
Ocean	16.7	2.3	27.7	4.2	27.6	3.6
Global	22.9	3.0	51.8	8.5	51.0	7.1

	mean	sdev	mean	sdev	mean	sdev
emissions						
North America	1.1	1.3	14.0	1.3	10.2	1.1
Central + South America	2.1	1.3	4.3	1.2	4.1	1.3
Africa	0.5	0.3	3.9	0.3	3.4	0.3
Europe	1.2	0.7	18.9	0.5	6.4	0.5
Former USSR + Middle East	0.3	0.3	9.6	0.3	8.1	0.3
Asia	1.8	1.0	10.2	1.0	16.7	1.1
Oceania	0.5	0.3	1.2	0.3	1.5	0.3
Continents	7.5	3.6	62.1	3.3	50.4	3.3
Ocean	21.0	10.0	30.2	11.0	30.2	10.0
Global	28.5	12.0	92.4	14.0	80.6	13.0
Number of models	7		6		7	

Table S4a. Multi-model mean and standard deviation regional deposition and emission (Tg(S)/yr) from SO<sub>x</sub> emissions for the historical period.

	2030					
	RCP26		RCP45		RCP85	
dry deposition	mean	sdev	mean	sdev	mean	sdev
North America	1.0	0.3	1.5	0.4	2.0	0.4
Central + South America	1.1	0.3	1.0	0.4	0.9	0.2
Africa	2.0	0.4	2.7	0.5	2.4	0.4
Europe	0.6	0.2	1.0	0.3	0.8	0.2
Former USSR + Middle East	1.8	0.3	2.7	0.5	3.2	0.5
Asia	6.3	1.2	7.4	1.8	9.0	1.4
Oceania	0.3	0.1	0.5	0.2	0.3	0.1
Continents	13.0	2.6	16.9	4.1	18.6	3.1
Ocean	10.7	5.2	14.5	7.8	12.5	5.7
Global	23.8	7.4	31.3	12.0	31.1	8.1

	mean	sdev	mean	sdev	mean	sdev
wet deposition						
North America	1.3	0.4	1.9	0.2	2.2	0.4
Central + South America	1.8	0.3	2.0	0.0	1.6	0.2
Africa	1.9	0.2	2.6	0.2	2.2	0.2
Europe	0.6	0.1	1.0	0.1	0.8	0.1
Former USSR + Middle East	1.8	0.1	3.1	0.5	2.9	0.3
Asia	6.7	1.1	8.4	1.3	8.4	1.5
Oceania	0.5	0.1	0.6	0.1	0.5	0.1
Continents	14.6	1.5	19.7	2.3	18.7	2.1
Ocean	21.3	1.2	25.3	1.9	23.6	1.6
Global	36.0	2.7	45.1	4.2	42.3	3.7

	mean	sdev	mean	sdev	mean	sdev
emissions						
North America	2.7	1.6	3.7	0.0	5.0	1.6
Central + South America	3.8	1.1	4.6	0.4	3.0	1.1
Africa	3.7	0.2	5.5	0.0	4.2	0.2
Europe	1.6	0.6	2.5	0.3	2.1	0.6
Former USSR + Middle East	3.7	0.3	5.9	0.0	6.9	0.3
Asia	15.1	1.0	19.0	0.4	20.4	0.9
Oceania	0.7	0.2	1.5	0.0	0.8	0.2
Continents	31.3	3.1	42.7	0.2	42.5	3.0
Ocean	28.5	5.6	35.2	5.8	30.8	5.6
Global	59.8	7.9	77.9	5.6	73.3	7.6
Number of models	4		2		4	

Table S4b. Multi-model mean and standard deviation regional deposition and emission (Tg(S)/yr) from SO<sub>x</sub> emissions for 2030.

	2100					
	RCP26		RCP45		RCP85	
	mean	sdev	mean	sdev	mean	sdev
dry deposition						
North America	0.4	0.3	0.5	0.2	0.5	0.3
Central + South America	0.4	0.2	0.5	0.3	0.6	0.2
Africa	1.5	0.3	1.5	0.4	1.6	0.3
Europe	0.3	0.1	0.4	0.2	0.3	0.1
Former USSR + Middle East	0.5	0.2	0.7	0.2	1.2	0.2
Asia	1.0	0.3	1.4	0.5	1.8	0.4
Oceania	0.2	0.1	0.4	0.1	0.2	0.1
Continents	4.3	1.3	5.3	1.9	6.4	1.6
Ocean	7.9	4.4	10.3	6.4	9.1	5.2
Global	12.3	5.5	15.7	8.3	15.4	6.5

	mean	sdev	mean	sdev	mean	sdev
wet deposition						
North America	0.8	0.4	0.9	0.1	1.0	0.4
Central + South America	1.1	0.2	1.5	0.1	1.3	0.2
Africa	1.6	0.2	1.6	0.0	1.8	0.1
Europe	0.4	0.1	0.6	0.0	0.5	0.1
Former USSR + Middle East	0.9	0.1	1.1	0.1	1.4	0.1
Asia	2.4	0.3	2.9	0.3	3.3	0.4
Oceania	0.4	0.1	0.5	0.1	0.4	0.1
Continents	7.7	0.4	9.1	0.4	9.7	0.4
Ocean	16.6	0.6	18.6	0.7	18.6	1.0
Global	24.4	0.9	27.8	1.1	28.3	1.4

	mean	sdev	mean	sdev	mean	sdev
emissions						
North America	1.4	1.7	1.2	0.0	1.7	1.7
Central + South America	1.9	1.1	3.3	0.4	2.3	1.1
Africa	2.9	0.3	2.9	0.0	3.2	0.3
Europe	0.9	0.6	1.2	0.3	1.0	0.6
Former USSR + Middle East	1.0	0.4	1.3	0.0	2.6	0.4
Asia	3.2	0.9	4.7	0.5	5.2	0.9
Oceania	0.5	0.2	1.1	0.0	0.6	0.2
Continents	11.9	3.5	15.6	0.2	16.6	3.5
Ocean	25.3	5.5	30.1	5.7	27.0	5.6
Global	37.2	7.6	45.8	5.5	43.6	7.7
Number of models	4		2		4	

Table S4c. Multi-model mean and standard deviation regional deposition and emission (Tg(S)/yr) from SO<sub>x</sub> emissions for 2100.

NOy	historical			RCP2.6		RCP4.5		RCP8.5	
	1850	1980	2000	2030	2100	2030	2100	2030	2100
CESM-CAM-Superfast									
CICERO-OsloCTM2									
CMAM									
GEOSCCM									
GISS-E2-R									
GISS-E2-R-TOMAS									
MOCAGE									
NCAR-CAM3.5									
NCAR-CAM5.1									
STOC-HadAM3									
UM-CAM									
Total	10	10	10	6	6	4	4	7	7

NHx	historical			RCP2.6		RCP4.5		RCP8.5	
	1850	1980	2000	2030	2100	2030	2100	2030	2100
CESM-CAM-Superfast									
CICERO-OsloCTM2									
CMAM									
GEOSCCM									
GISS-E2-R									
GISS-E2-R-TOMAS									
MOCAGE									
NCAR-CAM3.5									
NCAR-CAM5.1									
STOC-HadAM3									
UM-CAM									
Total	5	5	5	3	3	2	2	3	3

SOx	historical			RCP2.6		RCP4.5		RCP8.5	
	1850	1980	2000	2030	2100	2030	2100	2030	2100
CESM-CAM-Superfast									
CICERO-OsloCTM2									
CMAM									
GEOSCCM									
GISS-E2-R									
GISS-E2-R-TOMAS									
MOCAGE									
NCAR-CAM3.5									
NCAR-CAM5.1									
STOC-HadAM3									
UM-CAM									
Total	7	6	7	4	4	2	2	4	4

Table S5. Compendium of models providing fields for deposition analysis. A filled rectangle indicates a time slice to which the specific model contributed.

Ice Core Site Name	Latitude	Longitude	Elevation (m)
Antarctica			
W10	66° 44' S	112° 50' E	1390
THW	76° 57' S	121° 13' W	2020
DIV	76° 46' S	101° 44' W	1329
WD	79° 28' S	112° 41' W	1759
PIG	77° 57' S	95° 57' W	1593
NUS Site8_7	74° 53' S	01° 36' E	2700
NUS Site8_4	82° 49' S	18° 54' E	2552
NUS Site8_5	82° 38' S	17° 52' E	2554
NUS Site7_7	82° 04' S	54° 53' E	3725
NUS Site7_5	78° 39' S	35° 38' E	3619
NUS Site7_2	76° 04' S	22° 28' E	3582
NUS Site7_1	73° 43' S	7° 59' E	3174
Northern hemisphere			
ACT11d	66° 28' N	46° 18' W	2296
D4	71° 24' N	43° 54' W	2766
Zoe	72° 36' N	38° 18' W	3258
NEEMS3	77° 26' N	51° 03' W	2454
Tunu	78° 01' N	33° 59' W	2213
McCall	69° 18' N	143° 48' W	2400
Akademii Nauk	80° 31' N	94° 49' E	750
Flade Isblink	81° 35' N	15° 42' W	618

Table S6. Geographical information on the various ice-cores used in this study.

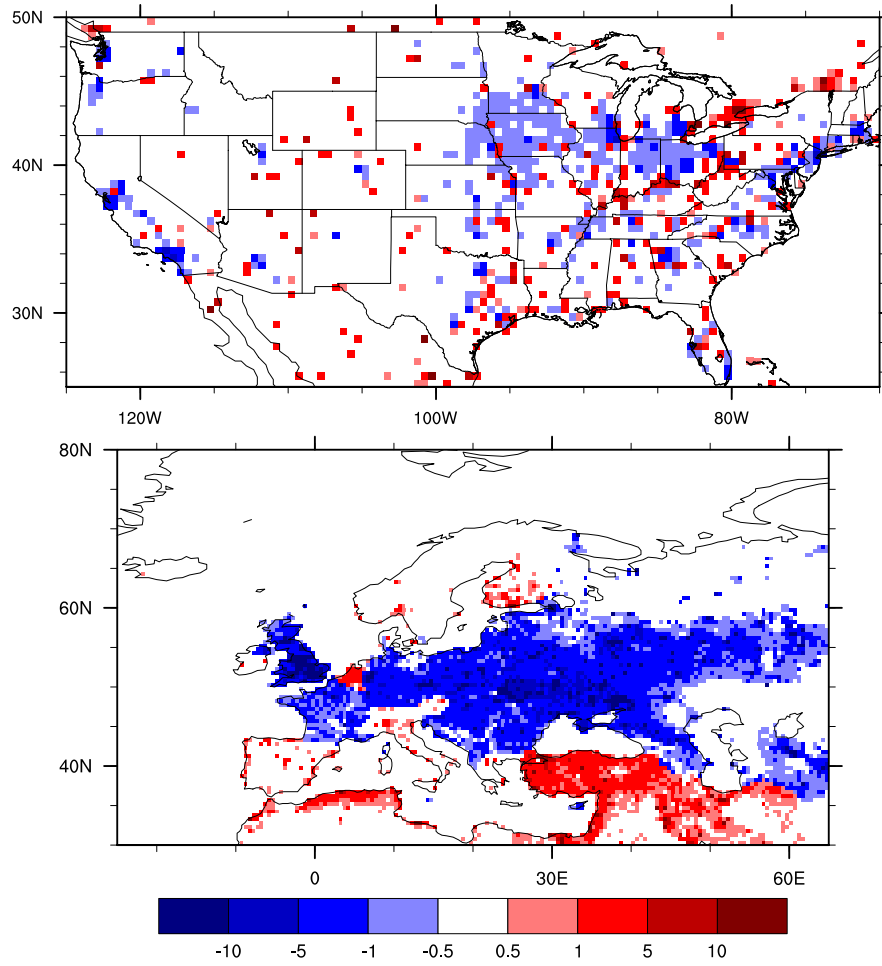


**Figure S1a.** Change in NO anthropogenic emissions (2000-1980) in  $10^{-2} \text{ mg(N)/m}^2/\text{year}$ .

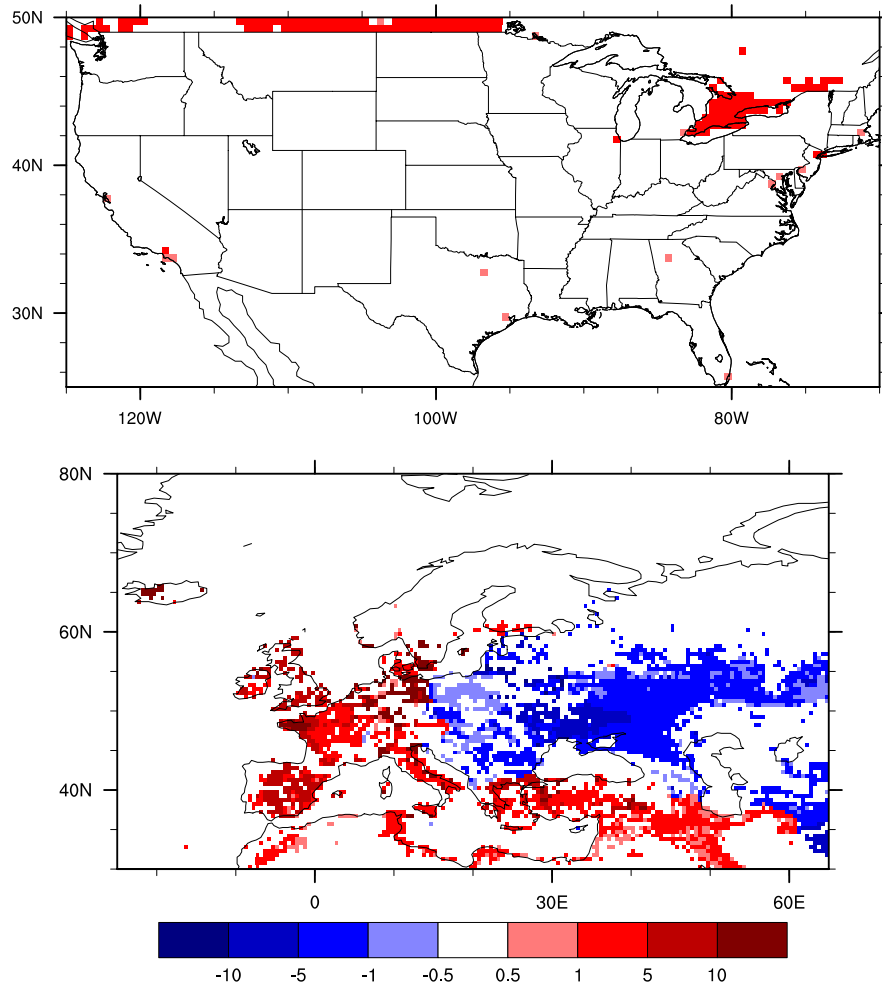


**Figure S1b.** Change in  $\text{NH}_3$  anthropogenic emissions (2000-1980) in  $10^{-2} \text{ mg(N)/m}^2/\text{year}$ .

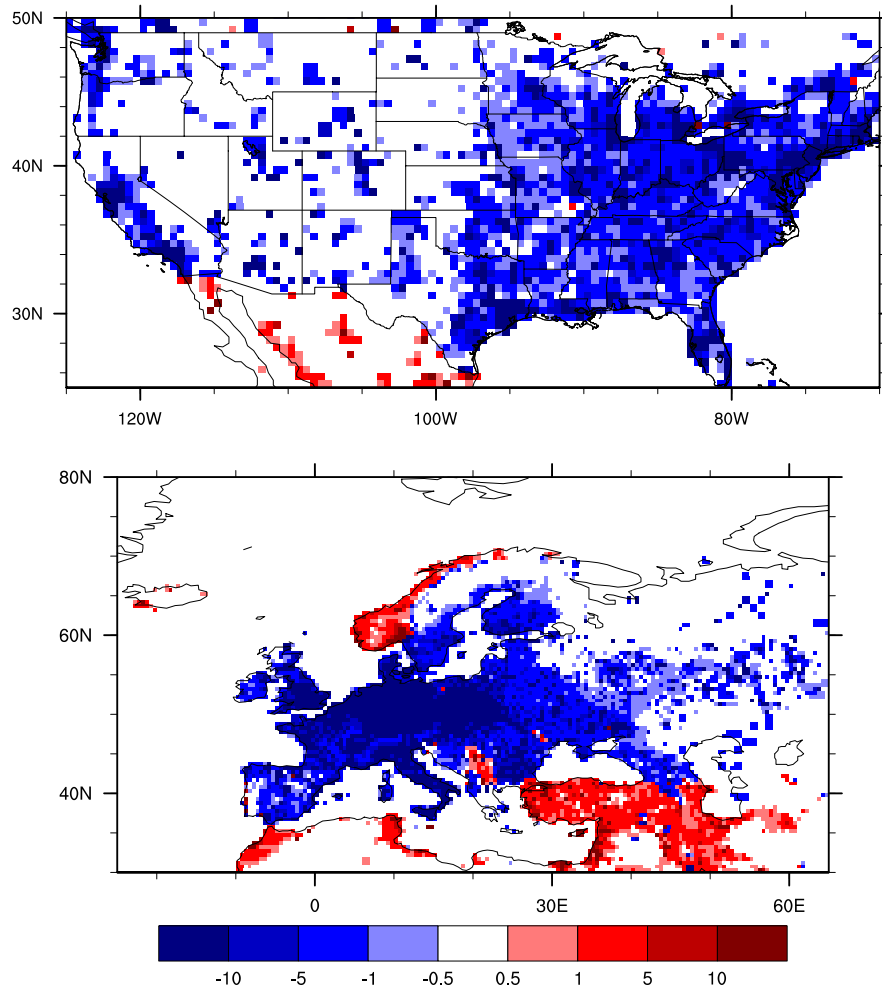


**Figure S1c.** Change in SO<sub>2</sub> anthropogenic emissions (2000-1980) in 10<sup>-2</sup> mg(S)/m<sup>2</sup>/year.

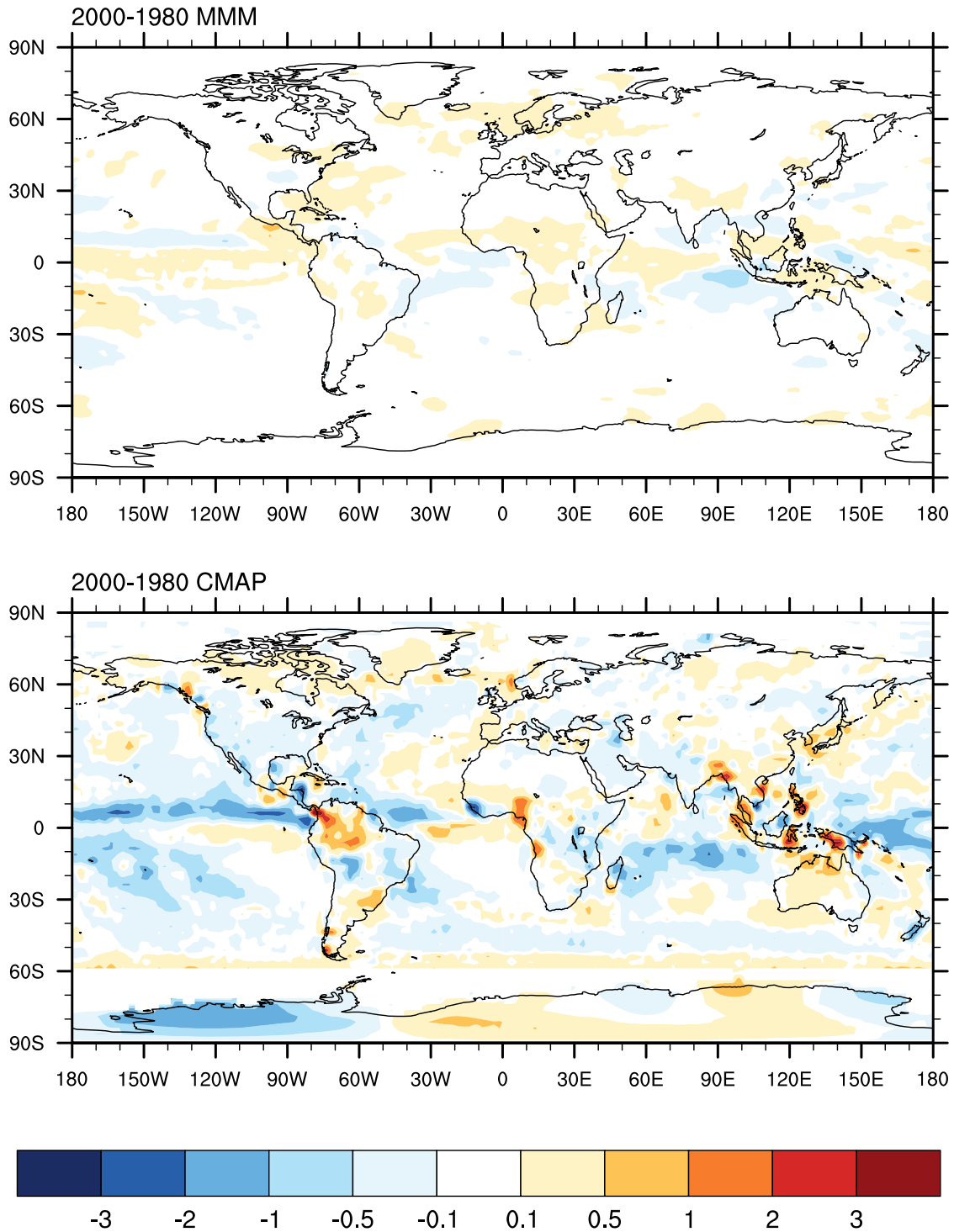


**Figure S2.** Comparison of annual mean precipitation (mm/day) change (2000-1980) from the ACCMIP MMM (top) and from the CMAP database (bottom; Xie and Arkin, 1997). Note that a 6-year average on the CMAP data is used for both time slices.

### Annual precipitation (mm/year)

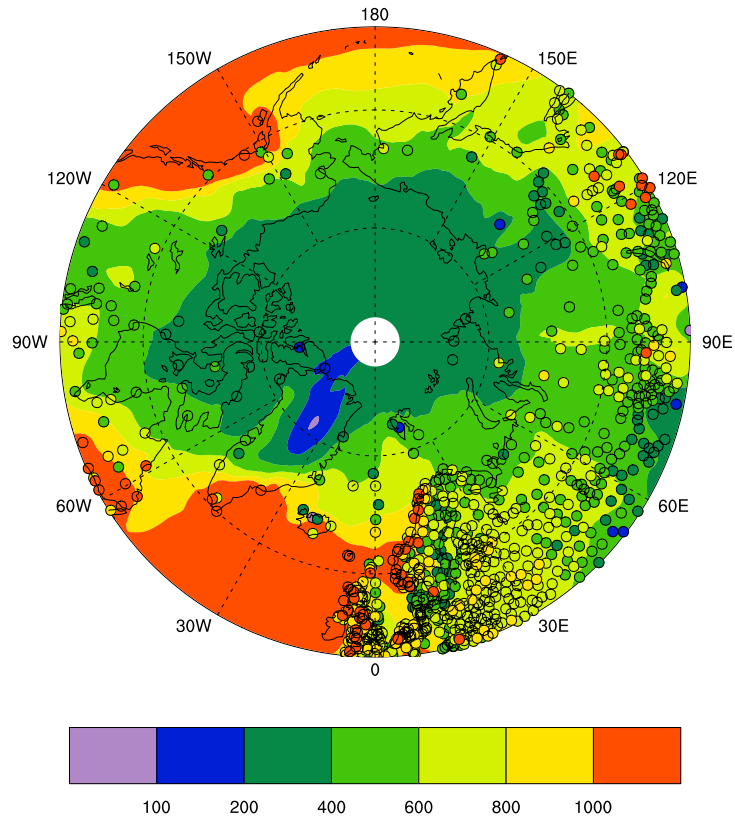


**Figure S3.** Annual mean precipitation from the ACCMIP 2000 MMM (contours) and observations (filled circles) from Yang et al. (2005).

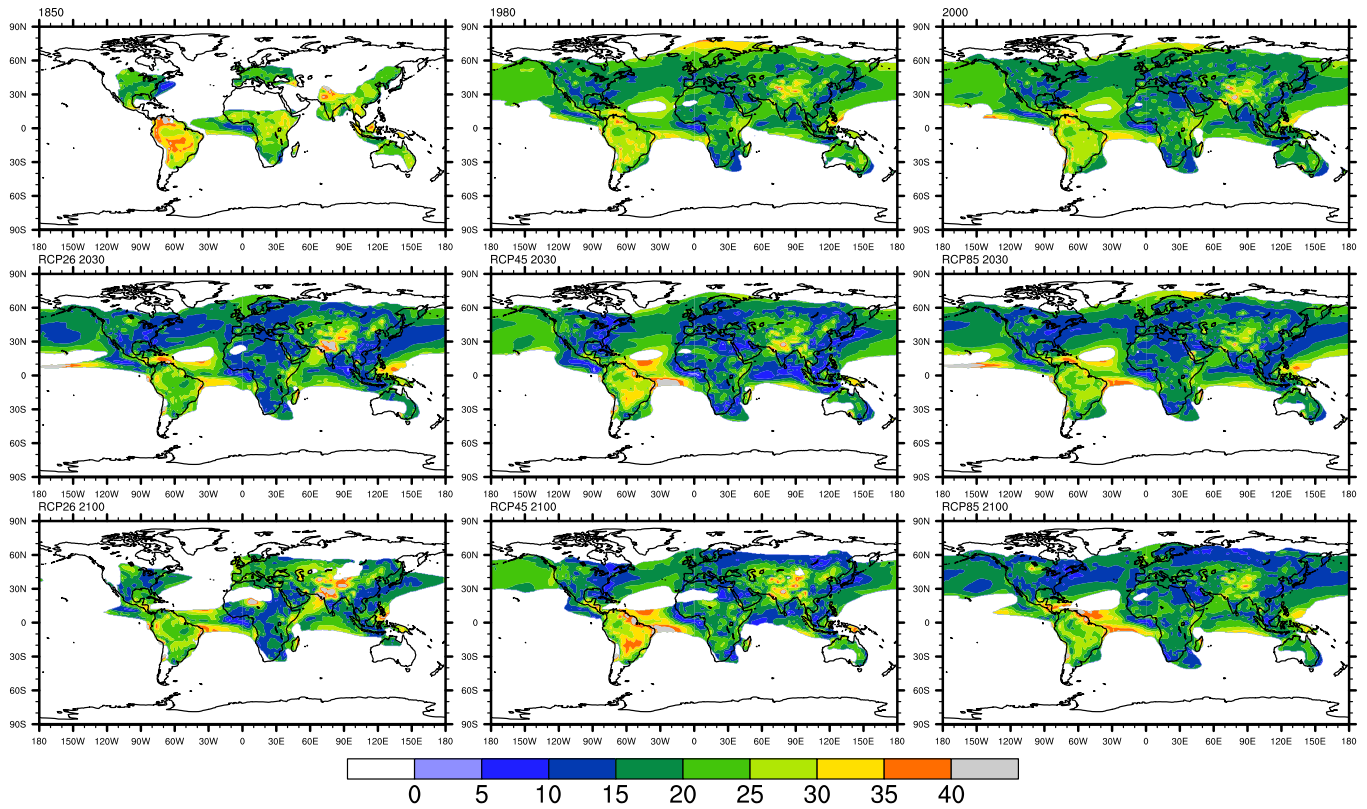


**Figure S4.** Inter-model standard deviation (in %) of the NO<sub>y</sub> wet deposition. The standard deviation is only shown for regions where deposition is larger than 50 mg(N)/m<sup>2</sup>/year (see Fig. 5a). The number of models used for each time slice is shown in Table S2.

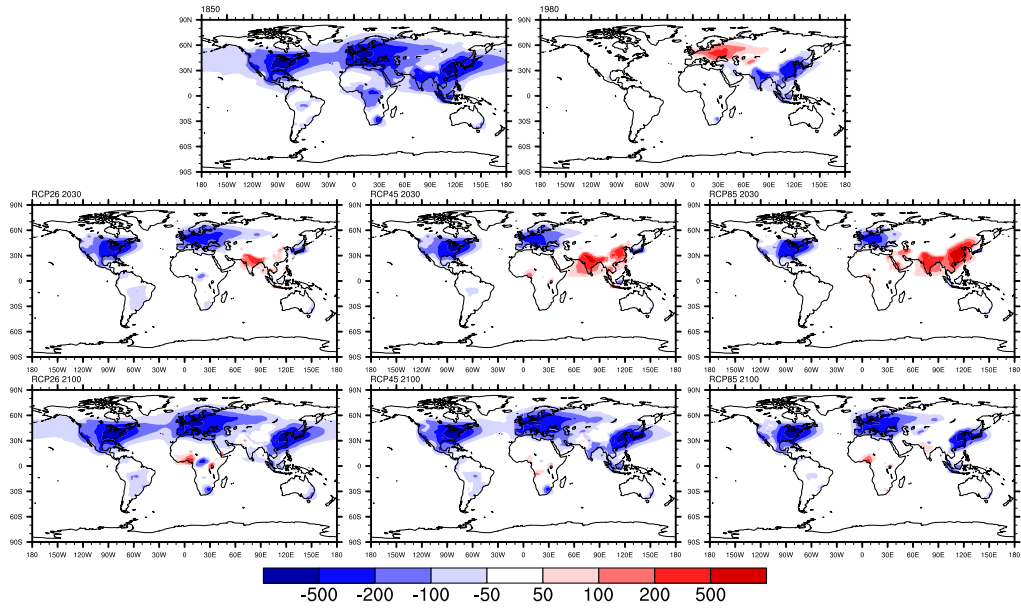


**Figure S5a.** Total (wet + dry) MMM NO<sub>y</sub> deposition 1850–2100 (mg(N)m<sup>-2</sup>yr<sup>-1</sup>) relative to year 2000. Top row shows 1850 and 1980. Middle row shows 2030 for RCP2.6, RCP4.5 and RCP8.5. Bottom row shows 2100 for RCP2.6, RCP4.5 and RCP8.5.

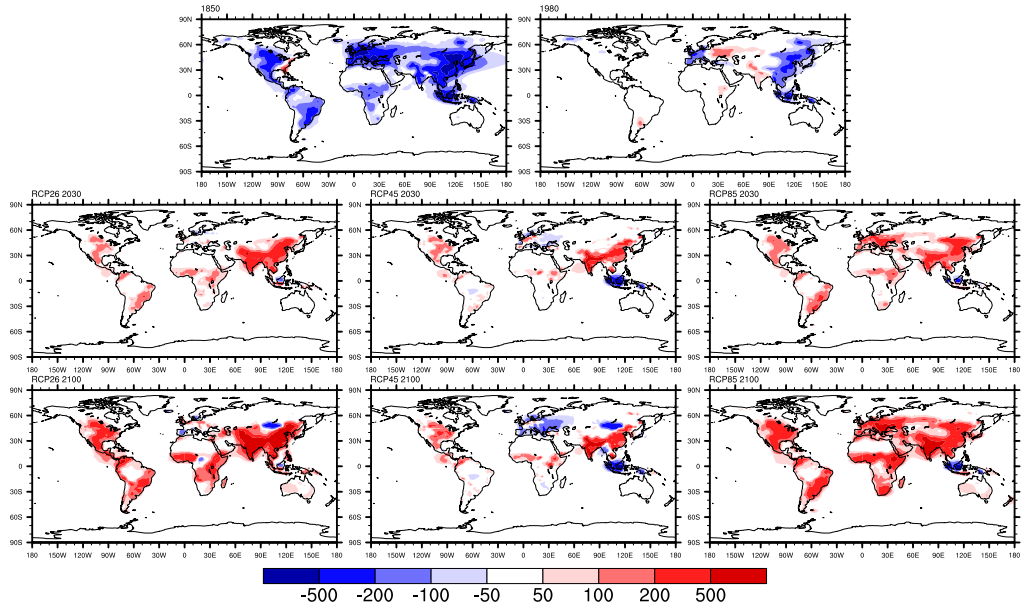


**Figure S5b.** Total (wet + dry) MMM  $\text{NX}_x$  deposition 1850-2100 ( $\text{mg(N)m}^{-2}\text{yr}^{-1}$ ) relative to year 2000. Top row shows 1850 and 1980. Middle row shows 2030 for RCP2.6, RCP4.5 and RCP8.5. Bottom row shows 2100 for RCP2.6, RCP4.5 and RCP8.5.

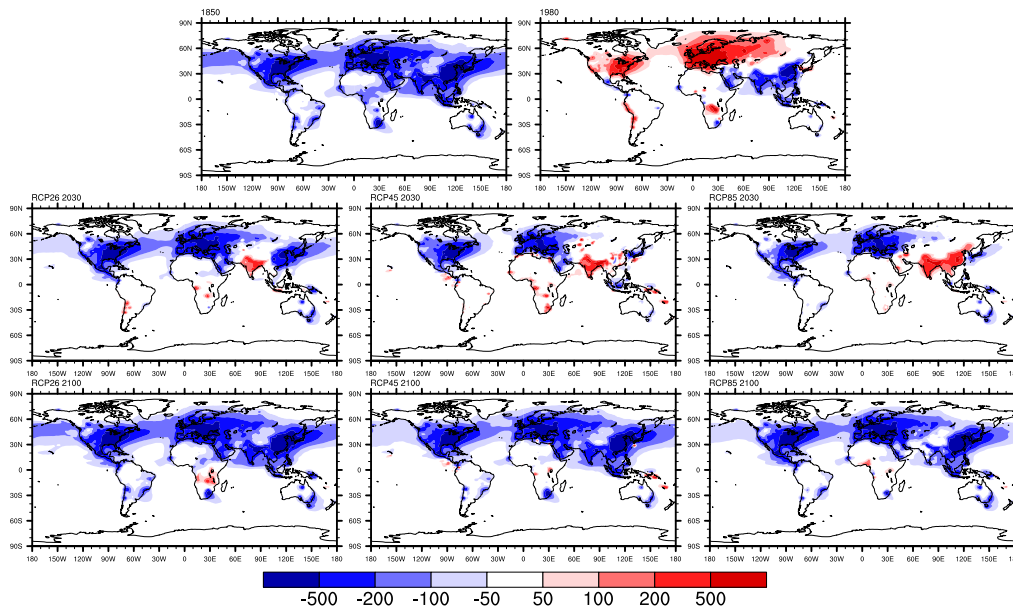


**Figure S5c.** Total (wet + dry) MMM SO<sub>x</sub> deposition 1850-2100 (mg(S)m<sup>-2</sup>yr<sup>-1</sup>) relative to year 2000. Top row shows 1850 and 1980. Middle row shows 2030 for RCP2.6, RCP4.5 and RCP8.5. Bottom row shows 2100 for RCP2.6, RCP4.5 and RCP8.5.